博士論文

ALTERED GLYCOLIPID METABOLISM AND ITS CELL BIOLOGICAL IMPACT IN PEROXISOMAL BIOGENESIS DISORDERS

(ペルオキシソーム形成異常症における糖脂質代謝変化と細胞機能への影響)

宮崎　セリーヌ
MIYAZAKI CELINE

ALTERED GLYCOLIPID METABOLISM AND ITS CELL BIOLOGICAL IMPACT IN PEROXISOMAL BIOGENESIS DISORDERS

A Dissertation

By

宮崎セリーヌ

Miyazaki Celine

41-117111

in Partial Fulfillment

of the Requirements for the Degree

Doctor of Philosophy

Advisor: Professor Masashi Mizuguchi

Co-Advisor: Dr. Makiko Saitoh

Development of Developmental Medical Sciences

Graduate School of Medicine

THE UNIVERSITY OF TOKYO

March 2014

TABLE OF CONTENTS

ABBREVIATIONS

(ATP)-binding	Adenosine triphosphate binding cassette transporter
ABC	ATP-binding cassette transporter
ACOX1	acyl-CoA oxidase 1 gene
ALDP	Adrenoleukodystrophy protein
CE	Cholesterol ester
Ch	Cholesterol
CHO-K1	Chinese hamster ovary K1 cells
CMH	Ceramide monohexoside
CDH	Ceramide dihexoside
CTH	Globotriaosylceramide
CNS	Central nerves system
D-PDMP	D-threo-1-phenyl-2-decanoylamino-3-morpholino-1-propanol
DBP	D-Bifunctional protein deficiency
DHAP-ATase	Dihydroxyacetonephosphate acyltransferase
DMSO	Dimethysulfoxide
FFAs	Free fatty acids
FITC	Fluorescein isothiocyanatedi
GalCer	Galactosylceramide
GD1a	Disialoganglioside GD1a
GD1b	Disialoganglioside GD1b
GlcGer	Glucosylceramide

GM1	Monosialotetrahexosylganglioside
GM3	Monosialoganglioside GM3
GNPAT	glyceronephosphate O-acyltransferase gene
H_2O_2	Hydrogen peroxide
HCl	Hydrogen chloride
IRD	Infantile Refsum disease
L-PDMP	L-threo-1-phenyl-2-decanoylamino-3-morpholino-1-propanal
LacCer	Lactosylceramide
LPC	Lyosphosphatidylcholine
LPE	Lysosphosphatidylethanlomine
MTT	3-(4,5-Dimethyl-2-thiazolyl)-2,5-diphenyl-2H-tetrazolium bromide
NALD	Neonatal adrenoleukodystrophy
PBDs	Peroxisome biogenesis disorders
PBS	Phosphate buffered saline
PC	Phosphatidylcholine
PS	Phosphatidylserine
PDs	Peroxisomal disorders
PE	Phosphatidylethanolamine
PEXs	Peroxisomal assembly peroxin genes
PMPs	Peroxisomal membrane proteins
PTS	Peroxisomal targeting signal protein
SEDs	Single peroxisomal enzyme deficiencies
SM1	Sphingomyelin 1
SM2	Sphingomyelin 2

TG	Triacylglycerol
TLC	Thin layer chromatography
UGCG	UDP-glucose ceramide glucosyltransferase
UGT8	Ceramide galactosyltransferase
VLCFAs	Very long chain fatty acids
X-ALD	X-linked adrenoleukodystrophy
ZS	Zellweger syndrome

LIST OF FIGURES

LIST OF TABLES

LIST OF PUBLICATIONS

1. Celine Miyazaki, Makiko Saitoh, Masayuki Itoh, Sumimasa Yamashita, Makoto Miyagishi, Sachio Takashima, Ann B. Moser, Masao Iwamori, Masashi Mizuguchi. (2013) "Altered phospholipid molecular species and glycolipid composition in brain, liver and fibroblasts of Zellweger syndrome." Neurosci Lett **552**(1):71-75.

GENERAL INTRODUCTION

Zellweger syndrome [OMIN#214100] (ZS) is an autosomal recessive disorder characterized by multi-organic clinical phenotypes: severe neurologic dysfunction, craniofacial abnormalities and liver dysfunction. It is characterized biochemically by the absence of peroxisomes. The incidence of ZS is estimated around 1/50,000 [Gould et al., 2001]. Most of the patients with classical ZS die within the first year of life [Wanders, 2010]. ZS belong to a group of peroxisomal disorders, which can be classified into two main groups: (1) peroxisome biogenesis disorders (PBDs) and (2) single peroxisomal enzyme deficiencies (SEDs). PBDs are classified into 4 main categories. Three of them, ZS, neonatal adrenoleukodystrophy (NALD), and infantile Refsum disease (IRD), consist a spectrum of overlapping phenotypes, with the severest being ZS and the mildest IRD. The remaining one, rhizomelic chondrodysplasia punctata, is distinguished from the other three by its unique phenotype.

Causative genes for PBDs, *PEX*s*,* encode peroxins, proteins essential for the biogenesis of peroxisome. ZS, NALD and IRD are genetically heterogeneous disorders resulting from mutations in any of the 12 *PEX*s. Rhizomelic chondrodysplasia punctata is caused only by mutations in *PEX7* [Gould et al., 2001].

The absence of peroxisomes in ZS patients results in various abnormalities in the metabolism of lipids including fatty acids, plasmalogens, cholesterol and bile acids. Tissues and cells originated from ZS patients have accumulation of very long chain fatty acids (VLCFAs) such as lignoceric (C24:0) or hexacosanoic (C26:0) acids, and branched chain fatty acids such as pristanic and homophytanic acids. These fatty acids are normally β-oxidized in peroxisomes. Plasmalogen is an ether-phospholipid synthesized by the enzymes localized in peroxisomes, and is decreased in patients with ZS [Gould et al., 2001].

Neurological deficits in ZS are caused by severe disturbance in brain development, characterized by impaired neuronal migration and hypomyelination. Clinical symptoms are profound hypotonia, seizures and severe motor and mental developmental delay. The neuropathology of ZS indicates the importance of peroxisomal function in the maturation of the central nervous system (CNS).

The molecular basis of ZS neuropathology remains to be elucidated. It is unknown how the accumulation of VLCFAs and/or defect of plasmalogen associate with the pathogenesis of ZS brain. It has been suggested that peroxisomal dysfunction affects mitochondrial function and enhances oxidative stress [Hein et al., 2008]. VLCFAs accumulation alone is not the sole cause for neuronal deficit in ZS, since normalization of the VLCFAs level in brain of *pex* knockout mice do not lead to a full restoration [Janssen et al., 2003]. In this study, I hypothesized that secondary metabolic alteration may be involved in the pathological brain development.

Accumulation of glycolipids has previously been noted in the cerebral grey matter, fibroblasts of ZS, as well as in peroxisome deficient mutant cells (Z65) [Saito et al., 1999]. Based on this finding, I focused on the secondary abnormalities in glycolipids metabolism. It is known that glycolipids are abundant in CNS and are involved in cellular proliferation, differentiation and recognition [Inokuchi, 2009]. Based on these facts, I speculated that glycolipids metabolism alternation could affect cellular signaling in neuronal migration process.

In the first chapter, I examined PBDs patients' tissues to confirm the accumulation of glycolipids in ZS. To elucidate how the accumulation of VLCFAs and/or the defect of plasmalogen is associated with the altered glycolipids metabolism, I analyzed the expression of glycolipid metabolizing enzymes using RNAi of peroxisomal enzymes. In the second chapter, in order to investigate the effects of accumulated glycolipids on cellular function, I

treated Z65 with a UDP-glucose glucosyltransferase inhibitor, D-PDMP. It has been shown that Z65 cells exhibit glycolipids accumulation such as glucosylceamide and GM3 ganglioside [Saito et al., 1999]. The objective of the present study is to elucidate how accumulated glycolipids affect cellular function in Z65, and how they are involved in the pathomechanism of ZS.

CHPATER 1

ALTERED LIPIDS COMPOSITION IN BRAIN, LIVER AND FIBROBLASTS OF PATIENTS WITH PEROXISOMAL DISORDERS

ABSTRACT

I studied the altered molecular species of lipids in brain, liver and fibroblasts from patients with Zellweger syndrome (ZS). ZS cerebellum samples contained a higher amount of sphingomyelin with shorter chain fatty acids compared to normal controls. The amount of phosphatidylethanolamine (PE) was smaller than a half of that in controls, with the absence of PE-type of plasmalogen. Gangliosides were accumulated in brain and fibroblasts of ZS patients. To investigate whether impaired beta-oxidation of very long chain fatty acids and/impaired plasmalogen synthesis affect glycolipids metabolism, RNAi of peroxisomal acyl Co-A oxidase (*ACOX1*) and glyceronephosphate O-acyltransferase (*GNPAT*), two enzymes involved in the first step of fatty acids beta-oxidation and plasmalogen synthesis, was performed using cultured neural cells. In neuronal F3-Ngn1 cells, *ACOX1* and *GNPAT* silencing up-regulated ceramide galactosyltransferase (*UGT8*) mRNA, and down-regulated UDP-glucose ceramide glucosyltransferase (*UGCG*) mRNA. These results indicate that both impaired beta-oxidation of VLCFAs and impaired plasmalogen synthesis affect glycolipid metabolism in neuronal cells.

1.1 INTRODUCTION

Function of peroxisomes

Peroxisomes are a single membrane bound organelle that contains various enzymes inside the peroxisomal matrix [Platta and Erdmann, 2007]. The localization and dynamics of peroxisomes vary depending on the cell type. Peroxins, proteins coded by *PEXs,* are essential for the biogenesis of peroxisomes (Fig. 1). *PEX*3 (OMIN 603164, chromosome 6q23-q24) and *PEX*19 (OMIN 600279, chromosome 1q22) are responsible for peroxisomal membrane proteins (PMPs) synthesis. *PEX*5 (OMIN 600414, chromosome 12p13) and *PEX*7 (OMIN 601757, chromosome 6q22-q24) are responsible for the import of peroxisomal matrix proteins. Peroxisomal enzyme proteins and integral peroxisomal membrane proteins are synthesized on free, cytoplasmic polyribosomes, and are imported from the cytoplasm through receptor-ligand binding. An important function of peroxisome is to catabolize VLCFAs such as hexacosanoic acid (C26:0) and tetracosanoic acid (C24:0) by peroxisomal ß-oxidation pathway [Wanders et al., 2007]. Other essential functions of peroxisomes are degradation of H_2O_2 and biosynthesis of ether-phospholipid, bile acid, cholesterol, and plasmalogens (Fig 2).

Peroxisomal disorders and etiology

Peroxisomal disorders (PDs) are caused by either the absence of proper peroxisomes or the deficiency of a particular peroxisomal enzymes [Steinberg et al., 2006]. The frequency of PDs is estimated to be 1 in 50,000 births [Gould et al., 2001]. PDs are inherited in an autosomal recessive manner except for X-linked adrenoleukodystrophy (X-ALD, OMIN

#300100). Patients with PDs have many overlapping phenotypes. Neurological dysfunction in PDs is severe and devastating. Abnormal development of the central nervous system (CNS) such as neuronal migration arrest is found in patients with PDs. The intrinsic role of peroxisomes in developing CNS is still poorly known [Janssen et al., 2003]. PDs are classified into two groups, peroxisomal biogenesis disorders (PBDs) and the single peroxisomal enzyme deficiencies (SEDs). In 1964, Zellweger and his colleagues were the first to describe cerebrohepatorenal syndrome, or Zellweger syndrome (ZS, OMIN#214100). Goldfischer et al. found in 1973 that peroxisomes are absent in ZS patients. Thereafter, ZS has been classified into PBDs. There are at least 13 *PEXs* identified to be responsible for PBDs. Mutations of *PEXs* result in the absence of detectable peroxisomal membrane structures or inability to recruit the matrix proteins into peroxisomes. Clinical phenotypes vary from severe to mild forms. The most severe clinical features are noted in ZS. Neonatal adrenoleukodystrophy (NALD) and infantile Refsum disease (IRD) reveal milder phenotype than ZS. Rhizomelic chondrodysplasia punctata (OMIN#215100) is characterized by chondrodysplasia, and is caused by *PEX7* mutation only (Fig.1). Treatments for patients with PDs are limited and only supportive.

SEDs include Acyl-CoA oxidase (ACOX, OMIN#264470) deficiency, D-bifunctional protein (DBP, OMIN#261515) deficiency and racemase (AMACR) deficiency (OMIN#604489). These enzyme are involved in the peroxisome β-oxidation pathway process to oxidize VLCFAs like tetracosanoic acids (C24:0) and hexacosanoic acid (C26:0). Acyl-CoA oxidase catalyzes at the first step of the β-oxidation process, and splits the long chains of fatty acids by two carbons until they are transferred to mitochondria for further oxidation [Wanders and Waterham, 2006]. ZS and DBP deficiency share severe neurological impairment [Barth et al., 2001, Faust et al., 2005, Gronborg et al., 2010]. For differential diagnosis between ZS and DBP deficiency, the amount of VLCFAs and plasmalogen are

screened. ZS patients show VLCFAs accumulation, a large amount of pipecolic acid and bile acid synthesis intermediates, and a small amount of plasmalogen [Wanders et al., 1987]. On the other hand, DBP deficiency impedes the oxidizing process of VLCFAs, resulting in the accumulation of VLCFAs in the plasma, but the level of plasmalogen is not affected [Ferdinandusse et al., 2006, Steinberg et al, 2004]. The mechanism of CNS abnormality in ZS and DBP deficiency is not yet clarified.

Candidate molecular basis of ZS neuropathology

The inability to form functional peroxisomes leads to malformation of brain, which reveals the importance of lipid metabolism in peroxisomes. However, it is still unclear to what extent the accumulation of peroxisomal substrates and/or deficiency of peroxisomal synthetic products contribute to CNS pathology in ZS. A potential mechanism could be oxidative stress, as this is known to be involved in other neurodegenerative diseases [Baes et al., 2012]. VLCFAs trigger oxidative damages in XALD model mice fibroblasts. However, the accumulation level of VLCFAs was not high in brain of these mice. The role of accumulated VLCFAs on neuropathology in ZS remains to be elucidated [Mullar et al., 2011].

Pathogenicity of the elevation of polyunsaturated fatty acids and dicarboxylic acids in ZS was raised. To identify metabolites as potential pathogenic factors in ZS, an unbiased metabolic profile is needed [Baes et al., 2012]. Our group has investigated altered lipid composition secondary to dysfunction of peroxisomes in peroxisomal deficient tissues and cells.

Our group previously reported an increase of ceramide monohexoside (CMH) and dipalmitoyl glycerophospholipids in the cerebral grey matter of a Japanese patient with ZS [Saitoh et al., 2007a]. In a DBP deficiency patient, lipid composition in white matter myelin, as well as the molecular species of plasmalogen-PE in the grey matter, was altered [Saitoh et al., 2008]. These altered molecular species were not directly induced by primary peroxisomal dysfunction, but may be secondary changes in the regulation of another metabolic pathway. In the present study, I conducted lipid analysis of ZS patients' brain, liver and fibroblasts to extend the previous findings.

Next, I hypothesized impaired peroxisomal β-oxidation and plasmalogen synthesis may modulate glycolipid synthesis via ceramide metabolism. Ceramides mediate apoptosis triggered by numerous mechanisms [Haynes et al., 2012]. Fatty acids including various chain lengths are bioactive molecules that reportedly exhibit *in vitro* anti-proliferative actions including induction of oxidative stress and modification of intracellular signaling pathway [Fauser et al. 2011]. Accumulated VLCFAs may induce the increase of ceramide, followed by the accumulation of CMH. To better understand the altered glycolipid metabolism in ZS patients' tissues, I here targeted glycolipid synthesizing enzymes expression by treating human neural cell lines with peroxisomal acyl-coenzyme A oxidase 1 (*ACOX1*) and glyceronephosphate O-acyltransferase (*GNPAT*) RNA interference (RNAi) (Fig. 4).

1.2 OBJECTIVE

The objective of this study is to observe altered lipid composition of ZS patients' postmortem tissues, brain and liver, and to investigate whether peroxisomal dysfunction causes glycolipid alteration in ZS patients' brain by using human neural cells.

1.3 MATERIALS AND METHODS

Control and patient samples

Six patients (ZS1-ZS5 and DBP) and six control (C1-C6) samples were examined in this study. Patients ZS1 (GM16866), ZS2 (101885), ZS3, ZS4 (GM13268) and ZS5 (GM13266) were diagnosed with ZS, and one patient (DBP) with DBP deficiency (Table 1). Patient GM16866 (ZS1) was a female with *PEX26* mutation who died at 6 months. Patient 101885 (ZS2) was a female with *PEX1* mutation who died at 7 months. Control GM5756 (C5) was a 6-years-old male who died of burns. Cerebellum and liver postmortem tissue samples from ZS1, ZS2 and C5 were obtained from the NICHD Brain and Tissue Bank at the University of Maryland in Baltimore, MD, USA. Fibroblasts samples (ZS4, ZS5, and C6) were provided by the Peroxisomal Diseases Laboratory, Kennedy Krieger Institute (Baltimore, MD, USA). Other postmortem tissues of cerebellum and cerebrum were obtained in Japan. ZS3 was a Japanese male patient with ZS who died at 7 months, and DBP was a patient with D-bifunctional protein deficiency who died at 1 year and 7 months [Saitoh et al., 2007a, 2008]. This study was approved by the Research Ethics Committee, Graduate School of Medicine and Faculty of Medicine, The University of Tokyo (No. 3188).

Total crude lipid extraction from tissue samples

Japanese patient samples were kept at -70˚C until use. The brain and liver tissues were put into the vacuum jar of a freeze-dryer for 8 h. The desiccated samples were weighted (dry weight). Lipid from each lyophilized cell pellets were extracted by adding 2 ml of chloroform/methanol/water (20:10:1 by volume) and incubated at 40˚C in a heat bath for 20 min. This procedure was done successively with other chloroform/methanol/water concentrations, (10:20:1 and 1:1:0, by volume), and the pooled lipid containing supernatant was added up to a total volume of 6 ml. Patient samples obtained from US were extracted by classic Folch method at the Kennedy Krieger Institute. Briefly, these brain and liver tissue samples were weighted and homogenized with chloroform/methanol (2:1, v/v). The extracted solution was separated into two phases after adding water equivalent to 20% volume of lipid solution. The lower phase of the solution was evaporated and the weight of the dried lipid was recorded. They were sent to our laboratory in a dried crude lipid form.

Thin layer chromatographylc (TLC) analysis for cholesterol, phospholipids, and glycolipids content.

After obtaining the crude lipid extracts from all the patients and controls, TLC analysis was performed. Glass capillary was used to aspirate the lipid. Then the lipid samples were gently applied on the silica gel TLC glass plates (Merck, Darmstadt, Germany). To ensure that all lipid samples from the tube were applied onto the TLC plate, 20 µl of (chloroform/methanol) (1:1, v/v) was added to the tube again. The diluted remaining lipid was reapplied to the same sample's spot. This application was done three times for all samples.

To consider cholesterol as the reference lipid in each sample that was extracted by different methods, cholesterol was quantified. Various known amounts of standard lipids were applied onto the same TLC plate along with the samples. The standard curve for

cholesterol ranged from 0.2 μg and 1.2 μg. TLC plate was developed for 20 min with solution for neutral lipids (hexane/diethyl ether/acetic acid) (80:20:1, v/v/v). Then, the plate was taken out to dry for 5 min. To visualize lipids, cupric acetate-phosphoric acid reagent was sprayed on the TLC plate first. Then the TLC plate was placed on a hotplate set at 170˚C until lipid spots appeared. After cooling, the plates were scanned. For lipid quantification, the intensity of lipid signal was meaaasured by Image J 1.42q software (NIH).

For phospholipids analysis, the standard curve was drawn from 0.4 μg and 1.4 μg. Chloroform/methanol/water (65:35:8, v/v/v) was used for developing the plate and the detection reagent, and temperature setting were the same as in cholesterol analysis. As for glycolipids analysis, the range of standard curve was from 0.2 μg to 1.2 μg. Chloroform/methanol/0.5% calcium chloride (60:35:8, v/v/v) was used for development, and the TLC plate was heated at 132˚C. Orcinol was used as the detection reagent.

Plasmalogen assay

To observe plasmalogen composition, the crude lipid samples from ZS patient's brain and liver were applied onto the TLC glass plates, and then they were immersed into the mobile (chloroform/methanol/water) (65:35:8, v/v/v) solvent. The lipid samples were adjusted to each 5 μg of PC and PE. PC and PE location was confirmed by the comparison to the standard visualized by cupric acetate reagent. The silicon coating involving PC and PE fraction was scraped out, and transferred to a 1.5 ml microtube. PC or PE containing silicon powder with 1 ml of chloroform/methanol (1:1, v/v) was heated at 40˚C for 20 min. The supernatant was aspirated and dried overnight. Chloroform/methanol (1:1, v/v) containing 0.05 M HCl was added and incubated for 40 min at 37˚C, followed by partition with water. HCl treatment cleaves the alkenly linkage in plasmalogen and generates lysophospholipid. The lower phase containing lysophospholipids was aspirated and prepared for TLC analysis.

HCl treated lipid samples were developed with chloroform/methanol/water (65:35:8, v/v/v). Cupric acetate-phosphoric acid reagent visualized the samples spots on the TLC plate at 170˚C.

TLC immunostaining for sphingomyelin (SM)

Total lipid extract equivalent to 2.0 μg of cholesterol was applied on the TLC plate. The TLC plates were developed by chloroform/methanol/water (65:35:8, v/v/v), dried, and subjected to 1.0% PVP/ 1.0% ovalbumin in PBS blocking buffer at 4 °C overnight. After blocking, the plates were incubated with a monoclonal mouse anti-sphingomyelin antibody (VJ-41, provided by Dr. Masao Iwamori) (1:500) in dilution buffer (3.0% PVP in PBS) at 37˚C for 2 h. After primary antibody incubation, the TLC plate was washed with 0.1% Tween 20 in PBS. Then, TLC plates were incubated with biotinylated anti-mouse IgG (H+L) secondary antibody (Vector Labs, CA, US) (1:1000) in dilution buffer (1.0% BSA in PBS) at room temperature for 30 min. After washing, avidin-biotin complex (ABC kit, Vector Labs, CA, US) was added to the TLC plates for 30 min with three times washing for staining. The lipid bands were visualized by 3,3'- diaminobenzidine (DAB) staining solution. (15 ml of distilled water/0.75 ml of 1.0 M Tris HCl (pH7.6)/3.0 mg of DAB/3.0 μl of 30% H_2O_2).

Neural cell culture

Human neuronal and glial cell lines were used. The neuronal cells were immortalized human neural stem cell clone of HB1.F3 transfected with neurogenin 1 transcription factor (F3-Ngn1) [Satoh et al., 2010]. The other cell type was human glioblastoma/astrocytoma cells (HTB-14). F3-Ngn1 cells were provided by Dr. Jun-ichi Satoh, Dept. of Bioinformatics, Meiji Pharmaceutical University, and HTB-14 cells were purchased from ATCC™ Biological Resource Center. F3-Ngn1 cells were cultured in DMEM media (Life

Thecnologies, CA, US) with addition of 10% heat inactivated fetal bovine serum and 2.0% penicillin/streptomycin. The media mixture was filtered through 0.22 μm membrane and stored at 4˚C before use. For HTB cells, MEM medium with 10% heat inactivated fetal bovine serum and 2.0% penicillin/streptomycin was used for culturing. F3-Ngn1 cells (3.0×10^6 cells per 25 cm^2 culture flask) in 4.0 ml of medium and HTB-14 cells (2.0×10^6 cells per 25 cm^2 culture flask) in 4.0 ml of medium were cultured in an incubator at 5.0% CO_2, 37˚C. Cells were harvested at 80% confluence with 0.05% trypsin. Then, the cells were transferred into a clean 15 ml tube and centrifuged at 1,000 rpm for 2 min. Supernatant was discarded and fresh 4.0 ml medium was add to the tube. Cells number per well was adjusted before seeding onto 6-well culture plates or culture bottles for shRNA transfection.

Vector preparation and transfection of *ACOX1* and *GNPAT* shRNA for fluorescence-activated cell sorting (FACS)

ACOX1 and *GNPAT* shRNA target sequences were designed by Dr. Makoto Miyagishi. Candidate sequences were chosen according to the predicted highest effectiveness. shRNA structure design contains bulged nucleotides that look like a hair pin [Moore et al., 2010]. The sequences were shown in Table 2. To incorporate green fluoresce protein (GFP) vector with *ACOX1* or *GNPAT* shRNA expression, GeneEraser pGE-2-hrGFP II shRNA Expression Vector Kit (Stratagene, CA, US) was used according to manufacturer's protocol (Fig. 5). Oligonucelotide sh*ACOX1* or sh*GNPAT* was inserted to the vector, and it was transformed to competent *E. coli.*, XL 10-Gold (Life Technologies), according to the protocol. The plasmid was extracted and purified by PureLink™ HiPure Plasmid Filter Purification Kits for Maxi preparation of Plasmid DNA (Life Technologies). A pre-constructed negative control vector (scrambled shRNA) was purchased from Stratagene, which included a random sequence. The cells in 6-well dish were transfected with 2.5 μg of

shRNA for 48 h using MultiFectam (Promega, Fichburg, US) according to manufacturer's protocol with optimal recommended transfection reagent volume (125 μl). Scrambled shRNA, sh*ACOX* and sh*GNPAT* transfected cells were treated with 0.05% trypsin. Trypsin was quenched with 3.0 ml of 10% dialyzed FBS in PBS buffer, and the cells were aspirated into a clean 15 ml tube and centrifuged at 1,000 rpm for 2 min. Supernatant was discarded, and the cells were re-suspended in a sorting buffer (PBS; 1.0 mM of EDTA/ 25 mM of HEPES (pH7.0)/ 1.0% of heat-inactivated and dialyzed FBS). GFP-positive cells were sorted and collected by flow cytometer BD FACSAria (Becton, Dickinson and Company, NJ, US) with 488-nm laser option. The FACS results were analyzed by BD FACSDiVa software. The collected GFP-positive cells were subjected to RNA extraction for RT-PCR analysis.

Polymerase chain reaction (PCR) condition

PCR was run by iCycler (Bio-Rad). AmpliTaq Gold (Life Technologies) was used to prepare PCR solution according to the manufacturer's manual. PCR conditions were as follows: 9 min at 95˚C followed by 35 cycles of 30 sec at 95˚C, 30 sec at 55˚C and 1 min at 72˚C, with a final elongation step of 7 min at 72˚C. Aliquots of PCR products were analyzed on a 2.0% ethidium bromide-stained agarose gel by electrophoresis.

Real-time quantitative polymerase chain reaction (RT-PCR) analysis

Total RNA was isolated from transfected cultures by TRIzol reagent (Life Technologies) according to manufacturer's instructions. Total RNA was reversely transcribed to cDNA by Ready-To-Go You-Prime First-Stand Beads first-stand cDNA synthesis kit (General Electric Company Healthcare, Buckinghamshire, UK) according to manufacturer's protocol. Random Primer (TAKARA BOI INC Shiga, Japan) was used. *ACOX1*, *GNPAT*, UDP-glucose ceramide glucosyltransferase (*UGCG*), ceramide galactosyltransferase (*UGT8*),

and glucose-6-phosphate dehydrogenase (*G6PDH*) gene expression was evaluated by using relative Quantification ABI PRISM® 7000 Sequence Detection System (Life Technologies). A total of 25 µl of each RT-PCR sample solution contained 10.5 µl water, 0.5 µl of DNA template, 0.75 µl each of forward and reverse primers, and 12.5 µl of Faststart Universal SYBR Green Master [ROX] (Roche, Basel, Switzerland). RT-PCR condition was 2 min at 50˚C, 15 min at 95˚C followed by 45 cycles of 30 sec at 95˚C, 30 sec at 53˚C and 1 min at 72˚C with final elongation step of 1 min at 95˚C and 30 sec at 53˚C. Primers for *ACOX1*, *GNPAT*, *UGCG*, *UGT8* and *G6PDH* were shown in Table 2.

Statistical analysis

Unpaired Student's *t* test was used to compare mRNA levels in samples from sh*ACOX* and scrambled shRNA or sh*GNPAT* and srambled shRNA. The p value <0.05 was considered significant. Data were obtained from at least three independent experiments. Values represented the mean±standard deviation (SD).

1.4 RESULTS

Cholesterol content determination in patient samples

Total lipid extract of 5.0 µl from cerebellum, and 10 µl from cerebral grey and white matter, were applied to TLC plate for analysis (Fig. 6). The cholesterol amounts in cerebellum and cerebral grey and white matter were determined (Table 3a and 3b, respectively). The same procedure was performed in 10 µl of total lipid from liver samples (Table 3c). Cholesterol ester (CE) contents in two ZS patients were slightly higher, but triglycerides (TG) and free fatty acids (FFAs) content differed from each other (Fig. 7). The cholesterol content in fibroblasts was also determined (Fig. 8) (Table 3d).

Phospholipid contents in ZS patients

Cerebellum lipid extracts relative to 2.0 μg of cholesterol from controls and patients were applied to TLC for phospholipid analysis (Fig. 9a). For liver samples, lipid extracts equivalent to 3.0 μg cholesterol were applied. Each phospholipid amount was compared between controls and patients' samples (Table 4). In the ZS1 and ZS2 patients, PE content in the cerebellum showed a decrease (Fig. 9a). Two types of sphingomyelin species, sphingomyelin 1 (SM1) and sphingomyelin 2 (SM2) were detected. SM1 appeared to be dominant in the cerebellum. To determine the exact ratio of SM1 to SM2 in each sample, TLC-immunostaining with anti-SM antibody was performed (Fig. 9b). In the cerebellum, an age-dependent increase of the ratio of SM1 to SM2 was shown in controls. The ratio of SM1 to SM2 was higher in ZS patients than in age-matched controls. In the liver of ZS1 and ZS2 patients, a decrease in PE content was also shown (Fig. 10a). While SM1 was dominant in the brain, SM2 was more abundant in liver samples. Unlike the cerebellum, SM1/SM2 TLC-immunostaining of the liver showed that the ratio varied in each patient (Fig. 10b). Bands indicated by arrows in Fig. 9a and Fig. 10a were detected in the patients' samples from both cerebellum and liver, respectively. The migration distances of these bands were close to those of FFAs.

Plasmalogen contents

The results from TLC analysis for phospholipids showed a decrease in PE and PC amount in the cerebellum; therefore, it is important to observe what kind of plasmalogen content may alter the proportion of the PE and PC in patients. Eight μg of PE and PC from total lipid of brain and liver were cleaved by HCl treatment. I could detect lysophosphatidylethanolamine (LPE) and lysophosphatidylcholine (LPC), derivatives of PE

and PC, respectively (Fig. 11). In both the ZS1 and ZS2 cerebella, PE-plasmalogen was not detectable (Fig. 11a), but PC- plasmalogen was found faintly in controls and in both patients indicated by an arrow (Fig. 11b). In both patients' livers, PE-plasmalogen did not appear after HCl treatment, but PC-plasmalogen appeared in all controls and patients (Fig. 12).

Altered glycolipid contents in tissues and cells from patients with ZS

Glycolipid composition in the ZS1 and ZS2 cerebella were analyzed (Fig. 13a). The bands of GM1 and GM2 gangliosides were hardly detectable for both the ZS1 and ZS2 samples. There were two unidentified materials closely located to GA1 and GM3 in the patients' samples, but not in the controls. The glycolipid composition in the frontal lobe grey and white matter from patients with ZS (ZS3) was shown in Fig.13b. The amounts of individual gangliosides in the grey matter of ZS3 patient were 1.2 to 1.4 times as much as those in the control. GM2 was detectable in the ZS3 grey matter, but not in the control brain. CMH and GT1b in the grey matter of ZS3 were increased compared to those in the control. The composition of the glycolipids was altered in DBP (Fig. 13b) as was previously described [Saitoh et al. 2008], but not in ZS3. Gangliosides, CMH, CDH and sulfatides were decreased in the grey and white matter in DBP. Then I investigated the glycolipid composition in lipid extracts derived from ZS2, ZS4, and ZS5 patients' fibroblasts. There was an increase in CDH, CTH, and GM3 compared to controls (Fig. 14). These findings were compatible with our previous data that CMH and gangliosides, such as GM3, are accumulated in PBD patients' fibroblasts [Tatsumi et al., 2001].

Lipid synthesis enzyme regulation in neural cells

I comfirmed the sequences of sh*ACOX1* and sh*GNPAT* inserted to the multiple cloning site of the GFP vector (Fig. 15). GFP-positive cells were observed by microscopy

(Fig. 16). The positive rates by immunofluorescence were 5.65% scrambled shRNA; 13.8% sh*ACOX1*; 10.5% sh*GNPAT* (values were accounted from the mean of 3 independent experiments) for F3-Ngn1 and 6.6% scrambled shRNA; 13.3% sh*ACOX1*; 15.9% sh*GNPAT* for HTB-14 cells, respectively (Fig. 17). Relative mRNA expression of *ACOX1* and *GNPAT* referenced to that of *G6PDH* was reduced to 0.274±0.055 and 0.196±0.044, respectively, in F3-Ngn1 cells, and to 0.542±0.042 and 0.430±0.131 in HTB-14 cells. The value was 1.000 in the scrambled shRNA treated cells, the difference being statistically significant (p<0.05). *ACOX1* shRNA induced a significant increase of *UGT8* mRNA expression in F3-Ngn1 (p=0.03). *GNPAT* shRNA also induced up-regulation of *UGT8*, but the difference was not statistically significant (p=0.10). *UGCG* mRNA expression decreased significantly in F3-Ngn1 cells with both shRNA (Fig. 18a). In HTB-14 cells, both shRNAs did not affect the expression of glycolipids synthesizing genes, except for up-regulation of *UGCG* through *ACOX1* silencing (Fig. 18b).

1.5 DISCUSSION

This study revealed altered molecular species of phospholipids and glycolipids in the tissues and fibroblasts of five ZS patients. A slight increase of cholesterol ester was noted in the liver of two ZS patients. The increase of cholesterol esters in PDs specimens was reported in previous studies [Saito et al., 2007a, Saitoh, et al. 2008]. Increased VLCFAs may be metabolized to cholesterol ester. Actually, increased cholesterol ester included very long fatty acyl moieties in the brain of patients with X-ALD [Brown et al., 1983].

Molecular species of SM modulate the stability of sphingolipid-enriched membrane microdomains that plays a role in the sorting and trafficking of membrane proteins [Smaby et al., 1996]. In the ZS1 and ZS2 cerebella, the ratio SM1 to SM2 was elevated, implying that

membrane protein sorting and trafficking may be affected in ZS. An increase of sphingomyelin with VLCFAs moiety in *pex*5$^{-/-}$ knockout newborn mice brain has been reported [Pettus et al., 2004]. In this study, sphingomyelin with longer fatty acid moiety was dominant in liver with ZS. This could be explained by the fact that peroxisomes in the digestive organ have specific catalytic action, different from that in the brain [Kovacs et al., 2009]. The rescue of liver peroxisome reportedly normalized the CNS abnormality in *pex*5$^{-/-}$ mice, suggesting the importance of metabolites relevant to liver peroxisomal function [Janssen et al., 2003].

The decrease in PE fraction in patients' specimens may reflect the decrease of PE-type plasmalogen. In mammals, the distribution and composition of plasmalogens varies among different tissues [Brites et al., 2009]. Nervous system, kidney, and testis contain relatively high level of PE-type plasmalogen. PC-type plasmalogen is abundant in the heart and skeletal muscles. The liver has a very small amount of plasmalogens. Our group detected both types of plasmalogens in normal control liver, while PE-type plasmalogen was absent in patient tissues. The amount of PC was comparable between the controls and patients. In a previous study, the decrease of PE-type plasmalogen in ZS brain was compensated by the increase of polyunsaturated fatty acyl moieties [Saitoh et al., 2009]. Plasmalogens have been implicated in several biological processes. They play a role in affecting membrane fluidity, mediate signal transduction and protect against oxidative stress [Wanders et al. 2010]. More detailed analysis of the phospholipid molecular species in the liver is necessary in the future.

Gangliosides are sialic acid containing glycerosphingolipids and found abundantly in the brain, particularly in neuronal cell membranes around synapses [Haughey, 2010]. Gangliosides are known to play a role in neuronal growth, migration and maturation, neuritogenesis, synaptogenesis and myelination [McJarrow et al., 2009]. Figure 19 shows the summary of alteration in gangliosides composition in ZS and DBP deficiency patients' brain.

The results of my *ACOX1* and *GNPAT* shRNA study were inconsistent between neuronal F3-Ngn1 and astrocytic HTB-14 cells. A plausible explanation is that the regulation of glycolipid metabolism is different depending on the cellular type. Increased CMH in the frontal lobe grey matter of ZS, but not in the white matter (Fig. 13a), might reflect the regional differences in glycolipids metabolism of CNS. The accumulation of VLCFAs by itself was unable to modulate glycolipid metabolism because CMH did not accumulate in the DBP deficiency patient's brain (Fig.13a). *UGT8* mRNA up-regulated by *ACOX1* and *GNPAT* silencing in F3-Ngn1 cells may synergistically accumulate CMH in the ZS grey matter, although the effect of *GNPAT* silencing did not reach statistical significance in my study. The increase in *UGCG* mRNA expression is by *ACOX1* and *GNPAT* shRNAs may be ascribed to the accumulation of gangliosides in the ZS grey matter. The present study, on the other hand, demonstrated down-regulation of *UGCG* by *ACOX1* and *GNPAT* shRNAs. According to a previous study, DNA damage with mitomycin C down-regulates *UGCG*, thereby increasing ceramides and up-regulating *UGT8* [Haynes et al., 2012]. These findings are consistent with my current results of *ACOX1* and *GNPAT* silencing. Although my findings were obtained from a limited number of samples, I suggest that peroxisomal dysfunction may affect glycolipids metabolism via ceramides metabolism in ZS.

1.6 CONCLUSION

I conducted lipid analysis in the brains, livers and fibroblasts of five ZS patients. The lipid composition in sphingomyelin, PE-type plasmalogens, gangliosides and neutral glycolipids were altered. Given the important roles of these lipids in cellular function, the present results may be relevant to the pathomechanism of peroxisomal disorders. The

disruption of the β-oxidation pathway and plasmalogen synthesis may affect glycolipid metabolism in the ZS brain.

CHAPTER 2

THE EFFECT OF ACCUMULATED GLYCOLIPIDS ON CELLULAR FUNCTION IN PEROXISOME-DEFICIENT Z65 CELL

ABSTRACT

The objective of this study is to elucidate whether accumulated glycolipids in peroxisome-deficient cells (Z65) are related to cellular functions including proliferation, viability to oxidative stress and cell adhesion. Incubating Z65 with an inhibitor of UDP-glucose glucosyltransferase, D-threo-1-phenyl-2-decanoylamino-3-morpholino-1-propanol (D-PDMP), reduced the amount of glucosylceramide (GlcCer) and gangliosides in Z65 and suppressed cellular proliferation. Our group had previously reported that Z65 were more fragile to H_2O_2 than wild-type cells (CHO-K1). D-PDMP aggravated fragility of Z65 to H_2O_2 exposure. In CHO-K1, fragility to H_2O_2 was not different between the treatments with L- and D-PDMP. Cell adhesion assay revealed that Z65 were more tightly bound to laminin or type IV collagen precoated plates than CHO-K1. Z65 expressed less binding to extracellular matrix molecules after D-PDMP treatment, suggesting that the accumulation of GlcCer and gangliosides affects cell adhesion. These data demonstrate that the accumulation of glycolipids in peroxisome-deficient cells alters multiple cellular functions, and may play a role in the pathogenesis of PBDs.

2.1 INTRODUCTION

Peroxisome biogenesis disorder and mutant *pex*2 cell model

Peroxisomal biogenesis is conducted by peroxins encoded by *PEX* genes. Peroxisomal matrix proteins are imported into the peroxisome from cytosol after binding to cargo receptors (Fig. 20). Mutations in *PEX* genes affect the biogenesis of peroxisomes, leading to various metabolic dysfunctions in the peroxisome. Mutant *pex2* cells (Z65) are peroxisome-deficient mutant cells isolated from wild type Chinese hamster ovary cells (CHO-K1) by mutagenesis [Tsukamoto et al., 1990]. Z65 are deficient in peroxisomal assembly, are unable to transport peroxisomal enzymes into the intracellular organelle matrix. This Z65 mutant model is used for studying the pathology in ZS, since CHO cells morphologically resemble normal fibroblasts and serve as a somatic cell model system [Tsukamoto et al., 1990, Spera, 2011] (Fig. 21).

Our group previously reported that Z65 show glycolipids accumulation compared to the wild type CHO-K1 [Saito et al., 1999, Saito et al., 2007b]. An autopsy case of ZS showed altered phospholipid species together with CMH accumulation in the brain tissue [Saitoh et al., 2007a]. GM3 is also accumulated in fibroblasts with ZS [Tatsumi et al., 2001]. In the chapter one of the present study, I showed that gangliosides and neutral glycolipids accumulate in ZS patients. Therefore, I hypothesized that these accumulated glycolipids could play pathogenetic roles in ZS by modulating cellular function. It is known that a proper amount of ganglioside is crucial in nervous system development, cell-cell transmembrane signaling, and membrane related protein function [Hakomori, 2002]. Mice with disrupted glycosyltransferase, responsible for ganglioside synthesis, exhibited neurodegeneration in the nervous system [Sugiura et al., 2005, Jennemann et al., 2005]. Neuronal cell differentiation and development are closely correlated to the biosynthesis and expression of gangliosides

[Varon et al., 1988]. The accumulation of gangliosides in peroxisome deficient cells could have affected neural migration during early developmental stage.

Z65 are useful peroxisomal deficient cells for evaluating cellular function by comparing them with wild type CHO-K1. Here, I hypothesize that the accumulation of glycolipids could alter various cellular functions. I assessed this hypothesis by investigating mutant Z65. I focused on cellular proliferation, fragility to H_2O_2 and cell attachment in mutant Z65 in the second chapter.

UDP-glucose glucosyltransferase inhibitor

D-threo-1-phenyl-2-decanoylamino-3-morpholino-1-propanal (D-PDMP) has an inhibitiory effect on UDP-glucose glucosyltransferase. The inhibitor acts as a ceramide analog for the substrate. It disrupts the downstream formation of more complicated gangliosides [Inokuchi, 2009]. On the other hand, the isomer L-threo-1-phenyl-2-decanoylamino-3-morpholino-1-propanal (L-PDMP) does not inhibit UDP-glucose glucosyltransferase. Since PDMP may show some cytotoxic effects [Inokuchi, 1997, 1998]. I used L-PDMP in this study as a reference of D-PDMP to eliminate the effects other than inhibition of UDP-glucose glucosyltransferase. (Fig.22).

2.2 OBJECTIVE

The objective of this study is to examine the effect of accumulated glycolipids on cellular proliferation, viability, and adhesion in peroxisome-deficient Z65 cells by using a UDP-glucose glucosyltransferase inhibitor, D-PDMP.

2.3 MATERIALS AND METHODS

Cell lines

CHO-K1 was obtained from JCRB Cell Bank (Osaka, Japan). The *pex*2 mutant cell line Z65 was provided by Prof. Yukio Fujiki, Department of Biology, Graduate School of Life Sciences, Kyushu University. Both CHO-K1 and Z65 were stored in liquid nitrogen before thawing. The cells were cultured at 37˚C in 5.0% CO_2 in DMEM/F12 (1:1) medium supplemented with 10% fetal bovine serum until it reached 80% to 90% sub-confluence.

Treatment with D- and L-PDMP

The standard glycolipids, GlcCer, lactosylceramide (LacCer) and ganglioside GM3, were purified from human erythrocytes. L- and D-PDMP were purchased form Matreya LLC (Pleasant Gap, PA, USA). I used the medium containing 30 μM D-PDMP according to a previous report [Inokuchi, 2009]. Both L- and D-PDMP were resolved by 100% of ethanol. PDMP solution was completely dried by lyophilization for 30 min, followed by addition of medium and sonication for 10 min. Cells were treated with 30 μM of L-PDMP or D-PDMP in medium, and were incubated for 48 h at 37˚C in 5.0% CO_2 incubator.

Lipid extraction and determination of glycolipid composition

CHO-K1 and Z65 were cultured in medium containing 30 μM L- or D-PDMP. After 48 h, cells were harvested with phosphate buffered saline (PBS) and transferred to a 15 ml tube. After centrifugation at 3,000 rpm for 5 min, the supernatant was discarded. The cells were washed with PBS and centrifuged again. After the pellet was made complete dry by lyophilization using manifold freeze-vaccum dryer for 8 h, the weight was measured.

Lipids from a lyophilized cell pellet were extracted by 200 µl of chloroform/methanol/water (20:10:1 by volume) and incubated at 40˚C in a heat bath for 20 min. This procedure was repeated twice with other chloroform/methanol/water concentrations, (10:20:1 and 1:1:0, by volume), and the lipid containing supernatant was pooled to a total volume of 600 µl. Two hundred µl of distilled water was added for partition by centrifuging at 3,000 rpm for 5 min. The lower phase of the solvent containing lipids was aspirated carefully, and was transferred to another 2 ml microtube. For glycolipid composition analysis, lipids extracted from 1.0 mg of dry weight cell pellet was applied onto TLC plates, and were placed in a glass chamber containing an appropriate mobile solvent chloroform/methanol/0.5% $CaCl_2$ (55:45:10, v/v). After the fractionation, the plates were sprayed with orcinol-H_2SO_4 reagent for visualization. The position of each lipid species was assigned using the corresponding standards. The intensity of each spot was measured with Image J software.

Effect of L- and D-PDMP on cell proliferation

The cells (7.8×10^3 cells per well) were seeded on a 24-well plate in the DMEM/F12 (1:1) medium supplemented with 10% fetal bovine serum medium. After 24 h, the medium was exchanged by the medium containing 30 µM of L- or D- PDMP, followed by incubation for 24, 48 and 72 h. The cells were harvested, and the cell number was counted.

Viability assay under H_2O_2 exposure

I investigated the effect of L- or D-PDMP treatment on the fragility to H_2O_2 exposure in both cells. The cells (1.0×10^4 per well) were cultivated on 96-well plates for 24 h in the DMEM/F12 (1:1) medium supplemented with 10% fetal bovine serum. Then the medium was exchanged with a medium containing 30 µM of L- or D- PDMP, followed by incubation

for 48 h. Then the medium was replaced by a medium containing 0 - 44 mM of H_2O_2. After 3 h exposure to H_2O_2, the medium was changed again with an ordinary medium. After 24 h, 0.1 mg of 3-(4,5-Dimethyl-2-thiazolyl)-2,5-diphenyl-2H-tetrazolium bromide (MTT) per well was added. After 4 h of incubation, the purple formazan was visible as precipitates. The supernatant was aspirated. Then, 200 µl of dimethysulfoxide (DMSO) was added to resolve the intracellular purple formazan. The absorbance of each well solution was measured at 490 nm by Model 680 microplate spectrophotometer (Bio-Rad, CA, USA). The optical density of solubilized formazan for cells without H_2O_2 was taken as 100% viability.

Cell adhesion assay

Laminin and fibronectin were purchased from Sigma Aldrich Co. (St. Louis, MO, US). Type IV collagen was obtained from Nitta Gelatin (Osaka, Japan). Laminin, fibronectin and type IV collagen were diluted to 10 µg/ml in PBS, and were added to an 8-well chamber slide glass plate (Lab-Tek II chamber slide, Nunc, NY, USA) for overnight at room temperature. Then the solution was replaced by 1.0% bovine serum albumin (BSA) in PBS. After incubation at 37 ˚C for 2 h, BSA solution was replaced by 100 µl of the warm assay medium (Dulbecco-modified MEM /F12 (1:1) supplemented with 1.0% FCS). Cells were harvested after 48 h incubation with L- or D-PDMP, and were re-suspended with the cold assay medium. For cell adhering procedure, 100 µl of cell suspension ($1.0x10^5$ cells/ml) was added to each well chamber containing 100 µl of the warm assay medium. The adherent cells were captured as they bind to the slides for 30 min at 37 ˚C in a humidified incubator containing 5.0% of CO_2. Then, the unbound cells were drained by from inverting the 8-well chamber slide glass to facilitate the removal of unbound cells and the media chambers. To fix the cells, the slide glass was washed in PBS, and then in 100% methanol for 90 sec with a

final immersion of PBS again. The fixed slide glass was left to dry and stained with Giemsa dye solution for 10 min. After the slide glass was washed and dried, the stained cells were quantified by counting at representative fields of 0.7mm^2 areas at a 100-fold magnification view.

Immunohistochemistry

Integrins mediate attachment to the extracellular matrix, and regulate the trafficking of lipid raft, which involves gangliosides on the cell membrane [Bridgewater et al., 2012, Todeschini et al., 2007]. I hypothesized that a decrease of glycolipids by D-PDMP treatment in Z65 may alter the expression and/ or localization of adhesion molecules such as integrins. CHO-K1 and Z65 (1.0×10^4 cells per well) were cultivated on an 8-well chamber slide glass for 24 h. Ordinary medium alone or medium containing 30 μM of L- or D- PDMP were replaced for 48h incubation at 37 ˚C in a humidified incubator containing 5.0% of CO_2. The cells were washed twice by PBS, and fixed by 4.0% paraformaldehyde/0.25% Triton X in PBS for 30 min at 4˚C. After fixation, the chamber slide glass was washed 3 times with 0.1% BSA in PBS. The cells were incubated with goat polyclonal anti-β1-integrin antibody (Santa Cruze) at 1:200 dilution with 1.0% BSA in PBS for 2h. The cells were washed with 0.1% BSA in PBS for 3 times and incubated with Alexa Fluor® 488 conjugated rabbit anti-goat IgM antibody (1:900 dilution) at room temperature for 60 min. The chamber slide glass was washed by 0.1% BSA in PBS and additionally washed by PBS. Cover glass was mounted on slide glass with a drop of Prolong Gold anti fade reagent (Life technologies, CA US). The cells were examined with a 100× oil immersion objective by a confocal laser scanning microscope (Olympus FluoView FV1000, Olympus, Tokyo, Japan).

Western blotting

CHO-K1 and Z65 were first incubated with L- or D-PDMP for 48 h in 75 cm^2 culturing bottle coated with 10 μg/ml of laminin, fibronectin and type IV collagen. The cells were collected and washed with PBS. Lysis buffer (1.0 M Tris-HCl, 1.0 M NaCl, 50 mM EDTA, 1:100 dilution of protease inhibitor mix (GE Healthcare, England, UK), and 1.0% Triton X) was added to the cell pellets. The cells were homogenized by gentle tapping, and were subjected to 10 sec sonication for 3 times. The cell lysate was centrifuged at 12,000 g for 30 min at 4.0˚C. The supernatant was transferred to a new microtube and the protein concentration was determined by bicinchoninic acid (BCA) assay using protein assays kit (Bio-Rad) according to the manufacturer's protocol. Each lysate was mixed with the same volume of 2.0×SDS sample buffer. Then the samples were heated at 95˚C for 2 min, and were immediately transferred to ice for cooling.

Each sample containing 40 μg of total protein was separated on an 8.0% polyacrylaminde SDS-PAGE gel. After electrophoreses, proteins were blotted on polyvinylidene difluoride (PVDF) membrane (Millipore, Billerica, MA, USA) that had been immersed to first in 99% methanol for 10 sec and then in transfer buffer (25 mM Tris-HCl pH7.6, 192 mM glycine, 0.03% SDS, 20% methanol), using Semi-dry blotting apparatus (Bio-Rad) at 1mA/1cm^2 constant current for 2 h.

The blotted membrane was blocked with 4.0% skim milk in PBS for 60 min at room temperature, and then incubated with goat polyclonal anti-β1-integrin antibody (1:200, Santa Cruze, CA, USA) in dilution buffer (5.0% BSA, 25 mM TBS, pH 7.4, 0.1% Tween 20) for overnight at 4.0˚C with gentle rotation. For ß-actin detection, the membrane was blocked with 4.0% skim milk in PBS for overnight at 4˚C, and was incubated with a mouse anti-ß-actin monoclonal antibody (1:500, Abcam, Cambridge, UK) at room temperature for 30 min. The membrane was washed twice with 0.1% Tween 20 in PBS and once with PBS for 5 min. The blots were incubated with a biotinylated rabbit anti-goat or mouse IgG (1:500) antibody

for β1-integrin or ß-actin, respectively, for 30 min. The blots were then incubated in ABC solution (Vector Lab, CA, USA) for 30 min at room temperature followed by washing for 4 times. Bound conjugates on the membrane were visualized with DAB staining solution (10 ml distill water, 0.75 ml 1.0 M HCl, pH7.6, 3.0 mg 3,3'-diaminobenzidine (DAB), 3.0 µl H_2O_2). The band intensity was measured by Image J 1.42 software.

Statistical analysis

Unpaired Student's *t* test was used for statistical analysis. The *p* value <0.05 was considered significant, unless otherwise stated. Data were obtained from at least three independent experiments. Values represent the mean±SD.

2.4 RESULTS

Alteration of glycolipids content by PDMP treatment in CHO-K1 and Z65

The amounts of gangliosides, GlcCer, CDH, CTH, GM2 and GM1 were larger than in Z65 comparing to CHO-K1 (lane Control of CHO-K1 and Z65 in Fig. 23 a and b, respectively). CHO-K1 with L−PDMP addition showed an increase in the amount of GlcCer and CDH compared to those without treatment (Control). (Fig. 23a). GlcCer, CDH, CTH, GM3, GM2 and GM1 gangliosides were expressed in L-PDMP-treated Z65 cells (Fig. 23b). D-PDMP-treatment induced a decrease of GlcCer in both CHO-K1 and Z65 (Fig 23a and b). CTH, GM3, GM2, and GM1 gangliosides were almost completely depleted in the D-PDMP-treated Z65. (Fig. 23b).

Effect on cellular proliferation

The cell number of Z65 was significantly larger than that of CHO-K1 at 48 h and 72 h (Fig. 24a). There was no significant difference in the cell number of CHO-K1 between L- and D- PDMP treatment (Fig. 24b). However, D-PDMP treatment significantly reduced the cell number of Z65 compared to L-treatment at 48 and 72 h (p=0.01 and 0.008, respectively) (Fig. 24c).

Cell viability and sensitivity towards H_2O_2

An important function in peroxisomes is to catabolize H_2O_2. Our group previously reported that Z65 was more fragile to H_2O_2 exposure than CHO-K1 [Saitoh et al., 2007b]. In this study, I analyzed whether D-PDMP treatment facilitates sensitivity towards H_2O_2 in Z65. When H_2O_2 concentration was less than 1.4 mM, CHO-K1 cells were able to resist to oxidative stress and maintain their viability (Fig 25a). As the H_2O_2 concentration exceeded 2.8 mM, the viability of the CHO-K1 declined rapidly. CHO-K1 showed no significant difference in cellular viability of CHO-K1 between L- and D-PDMP treatment. By contrast, Z65 with D-PDMP treatment showed a decline of viability at H_2O_2 concentration (0.34 mM) lower than that for CHO-K1 (Fig. 25b). At 1.4 mM H_2O_2 concentration, only 50 % of Z65 survived (Fig. 25b) whereas CHO-K1 showed 100% viability (Fig. 25a) with D-PDMP treatment. The difference of variability was significant between L- and D-PDMP treatment at H_2O_2 concentration of 2.8 mM (p<0.05) (Fig. 25b). D-PDMP, but not L-PDMP, rendered Z65 more fragile to H_2O_2 exposure.

Effect on cell adhesion

Cell adhesion on various extracellular matrixes was evaluated in CHO-K1 and Z65. Without treatment with L- or D-PDMP (control), Z65 were more tightly bound to laminin or type IV collagen coated plates than CHO-K1 (Fig. 26a), however, the difference between

CHO-K1 and Z65 did not reach statistical significance. CHO-K1 was more adhesive to fibronectin than Z65 under no treatment (Fig. 26a) with borderline significance ($p=0.06$). In CHO-K1, the difference of cell adhesion between L- and D- treatment in CHO-K1 was not significant (Fig. 26 b). In Z65, the adhesion to laminin, fibronectin and type IV collagen were significantly reduced by 30 μM D-PDMP treatment ($p<0.01$) (Fig. 26c). Taken together, D-PDMP affected cell adhesion in Z65, but not in CHO-K1.

Immunohistochemistry for ß1 integrin

I investigated the expression of ß1-integrin in CHO-K1 and Z65 by immunohistochemistry. Immunostaining indicated the presence of ß1-integrin on the entire surface of CHO-K1 and Z65 (Fig. 27). The staining intensity of ß1-integrin in Z65 was lower than that in CHO-K1 under control and L- or D-PDMP treatment. No difference of ß1-integrin staining intensity was shown between L- and D- PDMP treatment in both CHO-K1 and Z65.

Western blotting of ß1-integrin

The amount of ß1-integrin protein was significantly smaller in Z65 than in CHO-K1 under L- or D-PDMP treatment (Fig. 28a), consistent with the results of immnohistocemistry (Fig. 27). I determined he relative expression level of ß1-integrin normalized by the expression of beta actin in CHO-K1 and Z65 without PDMP treatment (control). The relative expression level of ß1-integrin in CHO-K1 was significantly higher than in Z65 without PDMP treatment ($p<0.01$) (Fig. 28b), as well as with L- or D-PDMP treatment ($p<0.01$, Fig. 28c).

2.5 DISCUSSION

My data showed that treatment with UDP-glucose glycosyltransferase inhibitor, D-PDMP, altered proliferation, viability under H_2O_2 stress, and adhesion to extracellular matrix molecules in Z65. CHO-K1 contained GM3 as their major ganglioside. Z65 contained various kinds of gangliosides synthesized from GM3, such as GM2 and GM1, which were decreased by D-PDMP treatment. L- PDMP increased ceramide dihexoside (CDH) in both CHO-K1 and Z65. The increase of CDH under L-PDMP treatment was previously reported in B16 melanoma cells [Inokuchi et al., 1997], consistent with the present study.

The proliferative functions of GlcCer on various cells have been shown [Akasako et al., 2011]. It is suggested that accumulated GlcCer in Z65 increases cellular proliferation. Inhibition of its synthesis by D-PDMP may reduce cellular growth. GlcCer serves as a basic precursor of other glycosphingolipids including GM3. Studies have shown that GM3 suppresses proliferation of various cancer cells [Wang et al., 2011]. However, gangliosides of the GM3 downstream, such as GD1a, disialyl ganglioside, and GD3, reportedly have proliferative effect on cells [Santos et al., 2011; Furukawa et al., 2012]. Therefore, simultaneous decrease of the downstream gangliosides may affect cellular proliferation of Z65 under D-PDMP treatment.

In the present study, the resistance to H_2O_2 exposure in CHO-K1 was not influenced by the GlcCer and/or gangliosides content. According to previous observation of our group, Z65 are more fragile to H_2O_2 exposure than CHO-K1 [Saito et al., 2007b]. The sensitivity of Z65 to H_2O_2 may partially be ascribed to a reduced amount of plasmalogen, which traps peroxide, and to an increase in polyunsaturated fatty acid sensitive to peroxide [Engelmann, 2004]. Accumulated GlcCer and/or gangliosides in Z65 have protective functions against peroxide, compensating for the loss of plasmalogen.

Pretreatment of Z65 with 30 μM D-PDMP resulted in a decrease in attachment to laminin, type IV collagen, and fibronectin compared to L-PDMP treatment. Z65 pretreated

with L-PDMP showed an increase of attachment to fibronectin alone compared to no treatment. The strength of attachment with different adhesion molecules reflects the cell surface adhesion receptors' signaling. Weaker β1-integrin expression in Z65 compared to that in CHO-K1 was shown by Western blotting. The difference between the amount of β1-integrin in CHO-K1 and Z65 was not changed after D-PDMP treatment. Therefore, the decrease of β1-integrin was not directly related to the accumulation of glycolipids in Z65 cells. Integrins are transmembrane receptors involved in cell signaling. They mediate cell attachment to the surroundings, and regulate cell cycle, cell shape and motility. Both ganglioside and β1-integrin are required for maintenance of plasma membrane microdomains, which may play crucial role in modulating integrin-mediated adhesion [Singh et al., 2010]. Under D-PDMP treatment, the decrease of gangliosides may alter the interaction of gangliosides and β1-integrin, affecting cell adhesion. Impaired cell adhesion may affect cell movements in the CNS with ZS. In this context, recent studies found that integrins, N-cadherin and astoactines are involved in neuron-neuron or neuron-glial adhesion during migration [Solecki, 2012]. Further investigation of altered interaction between gangliosides and β1-integrin observed in peroxisome deficient cells could provide better understanding of neuropathology in ZS.

2.6 CONCLUSION

This part of my research study provided evidence that accumulation of glycolipids in peroxisome-deficient cells affected cellular proliferation, viability to oxygen stress and cell adhesion, suggesting its role in the pathogenesis of peroxisome biogenesis disorders.

GENERAL SUMMARY AND FUTURE PLAN

In Chapter 1, I studied the altered molecular species of lipids in brain and liver tissues, and in fibroblasts from patients with ZS. ZS cerebellum showed a larger amount of sphingomyelin with shorter chain fatty acids and smaller amounts of PE compared to control cerebellum, as well as the absence of the PE-type of plasmalogen. Gangliosides were accumulated in the brain and fibroblasts of ZS patients. To investigate whether impaired beta-oxidation of very long chain fatty acids and/or impaired plasmalogen synthesis affects glycolipids metabolism, RNAi of *ACOX1* and *GNPAT* was performed using cultured neural cells. In neuronal F3-Ngn1 cells, *ACOX1* and *GNPAT* silencing up-regulated *UGT8* and down-regulated *UGCG*. These results suggest that both impaired beta-oxidation of VLCFAs and impaired plasmalogen synthesis affect glycolipid metabolism in neuronal cells.

In Chapter 2, I investigated whether accumulated glycolipids in peroxisome-deficient Z65 relates to the pathomechanism of PBDs. Treatment of D-PDMP reduced the amount of GlcCer and gangliosides in Z65 and suppressed cellular proliferation. Our group had previously reported that Z65 were more fragile to H_2O_2 than CHO-K1. D-PDMP aggravated fragility of Z65 to H_2O_2 exposure, suggesting protective effect of glycolipids against oxidative stress. Cell adhesion assay revealed that Z65 were more tightly bound to laminin or type IV collagen precoated plates than CHO-K1. Z65 expressed weak binding to extracellular matrix molecules after D-PDMP treatment, suggesting that the accumulation of GlcCer and gangliosides affects cell adhesion. I showed that the amount of β1-integrin in Z65 was smaller than in CHO-K1. Integrins mediate the formation of focal adhesions where integrins link to intracellular cytoskeletal complexes. These complexes play important roles in modulating cell adhesion and inducing cell shape changes involved in cell spreading and locomotion [Clark et al, 1995]. Integrins also regulate the trafficking of lipid raft (membrane

microdomain), which involves gangliosides on the cell membrane [Bridgewater et al., 2012]. Altered interaction of gangliosides and β1-integrin may affect cell adhesion, leading to impaired cell movements in the CNS with ZS (Fig. 29). Further investigation of altered interaction between gangliosides and β1-integrin in peroxisome deficient cells should provide better understanding of neuropathology in ZS.

In conclusion, the results of the present study provide evidence that accumulation of glycolipids in patients' tissues (Chapter 1) and their impact on cellular functions (Chapter 2), suggesting the pathogenetic role of accumulated glycolipids in the neuropathology of ZS.

REFERENCE

Akasako, Y., K. Nara, Y. Nagai and Y. Hashimoto (2011). "Inhibition of ganglioside synthesis reduces the neuronal survival activity of astrocytes." Neurosci Lett **488**(2): 199-203.

Baes, M. and P. P. Van Veldhoven (2012). "Mouse models for peroxisome biogenesis defects and beta-oxidation enzyme deficiencies." Biochim Biophys Acta **1822**(9): 1489-1500.

Barth, P. G., J. Gootjes, H. Bode, P. Vreken, C. B. Majoie and R. J. Wanders (2001). "Late onset white matter disease in peroxisome biogenesis disorder." Neurology **57**(11): 1949-1955.

Brites, P., P. A. Mooyer, L. El Mrabet, H. R. Waterham and R. J. Wanders (2009). "Plasmalogens participate in very-long-chain fatty acid-induced pathology." Brain **132**(Pt 2): 482-492.

Bridgewater, R.E., Norman, J.C., Caswell, P.T. (2012) "Integrin trafficking at a glance." J Cell Sci **125**(Pt 16):3695-3701.

Brown, F. R., 3rd, W. W. Chen, D. A. Kirschner, K. L. Frayer, J. M. Powers, A. B. Moser and H. W. Moser (1983). "Myelin membrane from adrenoleukodystrophy brain white matter--biochemical properties." J Neurochem **41**(2): 341-348.

Clark, E.A., Brugge, J.S. (1995) "Integrins and signal transduction pathways: the road taken." Science **268**(5208):233-239.

Engelmann, B. (2004). "Plasmalogens: targets for oxidants and major lipophilic antioxidants." Biochem Soc Trans **32**(Pt 1): 147-150.

Fauser, J. K., L. D. Prisciandaro, A. G. Cummins and G. S. Howarth (2011). "Fatty acids as potential adjunctive colorectal chemotherapeutic agents." Cancer Biol Ther **11**(8): 724-731.

Faust, P. L., D. Banka, R. Siriratsivawong, V. G. Ng and T. M. Wikander (2005). "Peroxisome biogenesis disorders: the role of peroxisomes and metabolic dysfunction in developing brain." J Inherit Metab Dis **28**(3): 369-383.

Ferdinandusse, S., M. S. Ylianttila, J. Gloerich, M. K. Koski, W. Oostheim, H. R. Waterham, J. K. Hiltunen, R. J. Wanders and T. Glumoff (2006). "Mutational spectrum of D-bifunctional protein deficiency and structure-based genotype-phenotype analysis." Am J Hum Genet **78**(1): 112-124.

Furukawa, K., K. Hamamura, Y. Ohkawa, Y. Ohmi and K. Furukawa (2012). "Disialyl gangliosides enhance tumor phenotypes with differential modalities." Glycoconj J **29**(8-9): 579-584.

Goldfischer, S., A. B. Johnson, E. Essner, C. Moore and R. H. Ritch (1973). "Peroxisomal abnormalities in metabolic diseases." J Histochem Cytochem **21**(11): 972-977.

Gould, S.J., G.V. Raymond, D. Valle (2001). The peroxisome biogenesis disorder. Scriver B.V., Beaudet S, Valle D, Sly O (Ed.), The metabolic and molecular basis of inherited disease, *MacGraw-Hill, New York*, 3181-3217

Gronborg, S., R. Kratzner, J. Spiegler, S. Ferdinandusse, R. J. Wanders, H. R. Waterham and J. Gartner (2010). "Typical cMRI pattern as diagnostic clue for D-bifunctional protein deficiency without apparent biochemical abnormalities in plasma." Am J Med Genet A **152A**(11): 2845-2849.

Hakomori Si, S. I. (2002). "The glycosynapse." Proc Natl Acad Sci U S A **99**(1): 225-232.

Haughey, N. J. (2010). "Sphingolipids in neurodegeneration." Neuromolecular Med **12**(4):

301-305.
Haynes, T. A., V. Filippov, M. Filippova, J. Yang, K. Zhang and P. J. Duerksen-Hughes (2012). "DNA damage induces down-regulation of UDP-glucose ceramide glucosyltransferase, increases ceramide levels and triggers apoptosis in p53-deficient cancer cells." Biochim Biophys Acta **1821**(7): 943-953.
Inokuchi, J. (2009). "Neurotrophic and neuroprotective actions of an enhancer of ganglioside biosynthesis." Int Rev Neurobiol **85**: 319-336.
Inokuchi, J., Y. Kuroda, S. Kosaka and M. Fujiwara (1998). "L-threo-1-phenyl-2-decanoylamino-3-morpholino-1-propanol stimulates ganglioside biosynthesis, neurite outgrowth and synapse formation in cultured cortical neurons, and ameliorates memory deficits in ischemic rats." Acta Biochim Pol **45**(2): 479-492.
Inokuchi, J., A. Mizutani, M. Jimbo, S. Usuki, K. Yamagishi, H. Mochizuki, K. Muramoto, K. Kobayashi, Y. Kuroda, K. Iwasaki, Y. Ohgami and M. Fujiwara (1997). "Up-regulation of ganglioside biosynthesis, functional synapse formation, and memory retention by a synthetic ceramide analog (L-PDMP)." Biochem Biophys Res Commun **237**(3): 595-600.
Janssen, A., P. Gressens, M. Grabenbauer, E. Baumgart, A. Schad, I. Vanhorebeek, A. Brouwers, P. E. Declercq, D. Fahimi, P. Evrard, L. Schoonjans, D. Collen, P. Carmeliet, G. Mannaerts, P. Van Veldhoven and M. Baes (2003). "Neuronal migration depends on intact peroxisomal function in brain and in extraneuronal tissues." J Neurosci **23**(30): 9732-9741.
Jennemann, R., R. Sandhoff, S. Wang, E. Kiss, N. Gretz, C. Zuliani, A. Martin-Villalba, R. Jager, H. Schorle, M. Kenzelmann, M. Bonrouhi, H. Wiegandt and H. J. Grone (2005). "Cell-specific deletion of glucosylceramide synthase in brain leads to severe neural defects after birth." Proc Natl Acad Sci U S A **102**(35): 12459-12464.
Kovacs, W. J., K. N. Tape, J. E. Shackelford, T. M. Wikander, M. J. Richards, S. J. Fliesler, S. K. Krisans and P. L. Faust (2009). "Peroxisome deficiency causes a complex phenotype because of hepatic SREBP/Insig dysregulation associated with endoplasmic reticulum stress." J Biol Chem **284**(11): 7232-7245.
McJarrow, P., N. Schnell, J. Jumpsen and T. Clandinin (2009). "Influence of dietary gangliosides on neonatal brain development." Nutr Rev **67**(8): 451-463.
Moore, C.B., Guthrie, E.H., Huang, M.T., Taxman, D.J. (2010) “Short hairpin RNA (shRNA): design, delivery, and assessment of gene knockdown.” Methods Mol Biol **29**:141-158.
Muller, C. C., T. H. Nguyen, B. Ahlemeyer, M. Meshram, N. Santrampurwala, S. Cao, P. Sharp, P. B. Fietz, E. Baumgart-Vogt and D. I. Crane (2011). "PEX13 deficiency in mouse brain as a model of Zellweger syndrome: abnormal cerebellum formation, reactive gliosis and oxidative stress." Dis Model Mech **4**(1): 104-119.
Pettus, B. J., M. Baes, M. Busman, Y. A. Hannun and P. P. Van Veldhoven (2004). "Mass spectrometric analysis of ceramide perturbations in brain and fibroblasts of mice and human patients with peroxisomal disorders." Rapid Commun Mass Spectrom **18**(14): 1569-1574.
Platta, H. W. and R. Erdmann (2007). "Peroxisomal dynamics." Trends Cell Biol **17**(10): 474-484.
Saito, M., M. Horikawa, Y. Iwamori, Y. Sakakihara, M. Mizuguchi, T. Igarashi, Y. Fujiki and M. Iwamori (2007b). "Alterations in the molecular species of plasmalogen phospholipids and glycolipids due to peroxisomal dysfunction in Chinese

hamster ovary-mutant Z65 cells by FABMS method." J Chromatogr B Analyt Technol Biomed Life Sci **852**(1-2): 367-373.

Saito, M., M. Iwamori, B. Lin, A. Oka, Y. Fujiki, N. Shimozawa, S. Kamoshita, M. Yanagisawa and Y. Sakakihara (1999). "Accumulation of glycolipids in mutant Chinese hamster ovary cells (Z65) with defective peroxisomal assembly and comparison of the metabolic rate of glycosphingolipids between Z65 cells and wild-type CHO-K1 cells." Biochim Biophys Acta **1438**(1): 55-62.

Saitoh, M., M. Itoh, S. Takashima, M. Mizuguchi and M. Iwamori (2009). "Phosphatidyl ethanolamine with increased polyunsaturated fatty acids in compensation for plasmalogen defect in the Zellweger syndrome brain." Neurosci Lett **449**(3): 164-167.

Saitoh, M., Y. Sakakihara, M. Mizuguchi, M. Itoh, S. Takashima, M. Iwamori, S. Kamoshita and T. Igarashi (2007a). "Increase of ceramide monohexoside and dipalmitoyl glycerophospholipids in the brain of Zellweger syndrome." Neurosci Lett **417**(2): 165-170.

Saitoh, M., S. Yamashita, N. Shimozawa, M. Mizuguchi and M. Iwamori (2008). "Changes in the amounts of myelin lipids and molecular species of plasmalogen PE in the brain of an autopsy case with D-bifunctional protein deficiency." Neurosci Lett **442**(1): 4-9.

Santos, A. X., J. E. Maia, P. M. Crespo, L. F. Pettenuzzo, J. L. Daniotti, F. M. Barbe-Tuana, L. M. Martins, V. M. Trindade, R. Borojevic and F. C. Guma (2011). "GD1a modulates GM-CSF-induced cell proliferation." Cytokine **56**(3): 600-607.

Satoh, J., S. Obayashi, H. Tabunoki, T. Wakana and S. U. Kim (2010). "Stable expression of neurogenin 1 induces LGR5, a novel stem cell marker, in an immortalized human neural stem cell line HB1.F3." Cell Mol Neurobiol **30**(3): 415-426.

Singh, R. D., D. L. Marks, E. L. Holicky, C. L. Wheatley, T. Kaptzan, S. B. Sato, T. Kobayashi, K. Ling and R. E. Pagano (2010). "Gangliosides and beta1-integrin are required for caveolae and membrane domains." Traffic **11**(3): 348-360.

Smaby, J. M., V. S. Kulkarni, M. Momsen and R. E. Brown (1996). "The interfacial elastic packing interactions of galactosylceramides, sphingomyelins, and phosphatidylcholines." Biophys J **70**(2): 868-877.

Solecki, D. J. (2012). "Sticky situations: recent advances in control of cell adhesion during neuronal migration." Curr Opin Neurobiol **22**(5): 791-798.

Spera, R. and C. Nicolini (2011). "CHO Proteome Alterations Induced by Reverse Transformation." Cell Biochemistry and Biophysics **61**(3): 731-737.

Steinberg, S., L. Chen, L. Wei, A. Moser, H. Moser, G. Cutting and N. Braverman (2004). "The PEX Gene Screen: molecular diagnosis of peroxisome biogenesis disorders in the Zellweger syndrome spectrum." Mol Genet Metab **83**(3): 252-263.

Steinberg, S. J., G. Dodt, G. V. Raymond, N. E. Braverman, A. B. Moser and H. W. Moser (2006). "Peroxisome biogenesis disorders." Biochim Biophys Acta **1763**(12): 1733-1748.

Sugiura, Y., K. Furukawa, O. Tajima, S. Mii, T. Honda and K. Furukawa (2005). "Sensory nerve-dominant nerve degeneration and remodeling in the mutant mice lacking complex gangliosides." Neuroscience **135**(4): 1167-1178.

Tatsumi, K., M. Saito, B. Lin, M. Iwamori, H. Ichiseki, N. Shimozawa, S. Kamoshita, T. Igarashi and Y. Sakakihara (2001). "Enhanced expression of a-series gangliosides in fibroblasts of patients with peroxisome biogenesis disorders."

Biochim Biophys Acta **1535**(3): 285-293.
Todeschini, A. R., J. N. Dos Santos, K. Handa and S. I. Hakomori (2007). "Ganglioside GM2-tetraspanin CD82 complex inhibits met and its cross-talk with integrins, providing a basis for control of cell motility through glycosynapse." J Biol Chem **282**(11): 8123-8133.
Tsukamoto, T., S. Yokota and Y. Fujiki (1990). "Isolation and characterization of Chinese hamster ovary cell mutants defective in assembly of peroxisomes." J Cell Biol **110**(3): 651-660.
Varon, S., B. Pettmann and M. Manthorpe (1988). "Humoral and surface-anchored factors in development and repair of the nervous system." Prog Brain Res **73**: 465-489.
Wanders, R. J., S. Ferdinandusse, P. Brites and S. Kemp (2010). "Peroxisomes, lipid metabolism and lipotoxicity." Biochim Biophys Acta **1801**(3): 272-280.
Wanders, R. J. and J. C. Komen (2007). "Peroxisomes, Refsum's disease and the alpha- and omega-oxidation of phytanic acid." Biochem Soc Trans **35**(Pt 5): 865-869.
Wanders, R. J. and H. R. Waterham (2006). "Peroxisomal disorders: the single peroxisomal enzyme deficiencies." Biochim Biophys Acta **1763**(12): 1707-1720.
Wanders, R. J. A., R. B. H. Schutgens, G. Schrakamp, J. M. Tager, H. Vandenbosch, A. B. Moser and H. W. Moser (1987). "Neonatal Adrenoleukodystrophy - Impaired Plasmalogen Biosynthesis and Peroxisomal Beta-Oxidation Due to a Deficiency of Catalase-Containing Particles (Peroxisomes) in Cultured Skin Fibroblasts." Journal of the Neurological Sciences **77**(2-3): 331-340.
Wang, P., S. Xu, Y. Wang, P. Wu, J. Zhang, T. Sato, S. Yamagata and T. Yamagata (2011). "GM3 suppresses anchorage-independent growth via Rho GDP dissociation inhibitor beta in melanoma B16 cells." Cancer Sci **102**(8): 1476-1485.

FIGURE LEGENDS

Figure 1

List of *PEXs* whose mutations give rise to multiple clinical symptoms in ZS and RCDP spectrum

PEXs encode peroxins, proteins play roles in peroxisomal membrane assembly, protein transport, and matrix protein transport. ZS spectrum is consists of ZS, NALD and IRD. ZS, Zellweger syndrome; NALD, neonatal neonatal adrenoleukodystrophy; IRD, infantile Refsum disease The remaining one, rhizomelic chondrodysplasia punctata (RCDP), is distinguished from the other three by its unique phenotype.

Figure 2

Peroxisomal membrane proteins and matrix import mechanism

Peroxisomal function includes various metabolic processes such as beta-oxidation of VLCFAs and biosynthesis of ether-phospholipids. The end product of peroxisomal ß-oxidation is shuttled to mitochondria.

Figure 3

Lipid structures and species.

Lipid species are consist of various headgroups and aliphatic chains composition. Phosphoglycerides and sphinomyelin are belonged to phospholipids. Glycolipids are abundant in the brain. The basic structure of glycosphingolipids consists of sugar chain and ceramide backbone. They are metabolized into many other forms of glycolipids.

Figure 4

Peroxisomal metabolic pathways.

Peroxisomal ß-oxidation involves oxidation of pristanic acid and VLCFAs. Plasmalogens are etherphospholipids, which are synthesized by DHAPAT and alkyl-DHAP synthase. To evaluate alteration of glycolipid metabolism by peroxisomal dysfunction, peroxisomal enzymes, *ACOX1* and *GNPAT*, were targeted for silencing by using RNAi system in human neural cells. *ACOX1*, acyl-CoA oxidase 1 gene; *GNPAT*, glyceronephosphate O-acyltransferase gene.

Figure 5

Schema of vector construction of pGE-2-hrGFP II shRNA

Expression vector was digested with *Xba I* and *BamH I* to allow directional insertion of shRNA. The vector was tranfected to the neural cells.

Figure 6

TLC analysis for cholesterol in controls' and patients' cerebellum and cerebrum of grey (G) and white (W) matter samples

Cholesterol (Ch) and free fatty acids (FFA) were detected in brain samples. The amount of cholesterol was shown in Table 3. The lipid bands located below Ch are phospholipids. (a), TLC of cerebellum; (b), TLC of cerebrum.

Figure 7

TLC analysis of cholesterol in controls' and patients' liver

Cholesterol, free fatty acids (FFA) and triacylglycerol (TG) were shown in liver samples. TG is expressed similarly in age-matched control of C4 and ZS1 samples. The amount of cholesterol ester (CE) is much higher in ZS1 than the control.

Figure 8
TLC analysis of cholesterol in controls' and patients' fibroblasts
Cholesterol was detected in all samples. The amount was shown in Table 3.

Figure 9
TLC analysis of phospholipids in controls' and patients' cerebellum
(a) PE expression decreases significantly in both ZS1's and ZS2's cerebellum. TLC immunostaining was performed to identify SM1 and SM2 using VJ-41 mouse anti-sphingomyelin antibody. (b) SM1 to SM2 ratio in ZS1 and ZS2 was determined. The amount of SM1 was higher than in age-matched controls (C1, C2 and C3). The band indicated by an arrowhead, is closed to the location of free fatty acid.

Figure 10
TLC analysis of phospholipids in controls' and patients' liver
(a) PE expression was lower in both ZS. The amount of SM2 was larger in ZS than in control (C4). (b) TLC immunostaining of SM1 and SM2 ratio distributions was different among patients and control. The band indicated by an arrowhead shows high amount of free fatty acid in ZS1's and ZS2's liver.

Figure 11
TLC assay for plasmalogen content before and after HCl treatment in controls' and patients' cerebellum
(a) LPE was absent in patients. (b) LPC was detectable in all controls and patients.

Figure 12
TLC assay for plasmagolen content before and after HCl treatment in controls' and patients' liver
(a) LPE was absent in patients. (b) LPC was found in both control and patients and was more abundant in liver than in cerebellum (Figure 11b).

Figure 13
TLC analysis of glycolipids in controls' and patients' cerebellum and cerebrum of grey and white matter
(a) Unidentified glycolipids in ZS1 and ZS2 (indicated by bold arrows) were closely located to GA1 and GM3. (b) Ceramide monohexoside (CMH) was accumulated in grey matter (lane G) of ZS3, but not in that of DBP. G, grey matter of cerebrum; W, white matter of cerebrum.

Figure 14
TLC analysis of glycolipids in controls' and patients' fibroblasts
GM3, as well as CDH and CTH were increased in ZS patients than in control.

Figure 15
shRNA vector construction
Transformed colonies of competent *E. coli* with shRNA were screened by PCR and subjected to sequence confirmation for *ACOX1* or *GNPAT* shRNA insertion.

Figure 16

A representative confocal laser microcopy picture of GFP positive transfected cells

GFP signal was observed in both cells. The intensity of GFP signal was lower in sh*GNPAT* transfected cells than in sh*ACOX1* transfected cells.

Figure 17

Sorting of F3-Ngn1 and HTB-14 cells transfected with scrambled shRNA

(a) Sorting of GFP-positive F3-Ngn1 cells. Sample plot of F3-Ngn1 cell populations shown in the scattergram (upper panel) were broken into two groups; cells that were GFP(+) (brown) and others (red). The histogram (lower panel) showed the cell number of cells sorted by the FITC intensity. (b) Sorting of HTB-14 cells. GFP (+) HTB-14 cells were presented in blue in the scattergram (upper panel). The number of GFP (+) HTB-14 cells was presented in the histogram (lower panel).

Figure 18

Relative expression of *UGCG* and *UGT8* in A*COX1* and *GNPAT* RNAi F3-Ngn1 and HTB-14 cells

Both *ACOX1* (black column) and *GNPAT* (grey column) silencing in F3-Ngn1 cells up- regulated *UGT8*, but not *UGCG*. In HTB-14 cells, expression of *UGT8* was not affected. Relative expression of scrambled shRNA (white column) was demonstrated as 1.00. *$p<0.05$, **$p<0.01$.

Figure 19

Summary of altered glycolipids composition in DBP and ZS patients

Glycolipids composition on TLC analysis was different between DBP and ZS patients' brain based. In all ZS patients' samples showed a high amount of CMH and/or gangliosides. Up-regulation of *UGT8* from *ACOX1* and *GNPAT* RNAi in F3-Ngn1 cells may suggest the accumulation of CMH in ZS patient's grey matter.

Figure 20

The import of peroxisomal matrix proteins through the peroxisome membrane assembly

PTS-proteins are bound to PEX5 or PEX7 proteins and guided to the docking site at the peroxisomal membrane. After translocation of the PTS-protein and PEX5 or PEX 7 complex to the luminal side of the membrane, the complex is disassembled to release the PTS-protein into the lumen, and the PEX5 or PEX 7 returns back to the cytosol.

Figure 21

***Pex2* mutant Chinese hamster ovary cells (Z65)**

Pex2 mutant Chinese hamster ovary cells (Z65) were isolated in 1990 by Tsukamoto T. Random mutation was generated from wild type CHO-K1. The entire candidate CHO-K1 mutants were screened. *Pex*2 mutant CHO-K1, Z65 was isolated. In Z65, assembly of the peroxisomes is defective and the synthesis of peroxisomal proteins is normal. Catalase was active in the normal CHO-K1, but not in Z65.

Figure 22

Structure of L-PDMP and its enantiomer, D-PDMP

D-PDMP inhibits GlcCer and LacCer synthase, but its isomer, L-PDMP does not. D-PDMP depletes endogenous glycosphingolipids. Z65 possess an abnormal high amount of GlcCer and GM3. D-PDMP is a suitable tool to study the roles of glycolipids accumulation and its impact on cellular function in Z65.

Figure 23

TLC analysis of glycolipids content for CHO-K1 and Z65

Total lipids extracted from 0.1mg of dry weight of cells were developed on TLC plates with chloroform/methanol/0.5% $CaCl_2$ (55:45:10, v/v) and then visualized with orcinol-H_2SO_4 reagent. (a) GlcCer in CHO-K1 showed an expected decrease after D-PDMP treatment, but with L-PDMP treatment, the amount of GlcCer and CDH increased. (b) Not only GlcCer but also gangliosides were decreased in Z65 with D-PDMP treatment, compared to no (control) or L-PDMP treatment. L-PDMP did not have inhibitory effect on glycolipids expression in Z65 cells.

Figure 24

Effect od L- and D-PDMP on CHO-K1 and Z65 proliferation

The comparison of cell numbers between CHO-K1 and Z65 under no treatment (a). At 48 h and 72 hr, the cell numbers of Z65 were significantly larger than those of CHO-K1.

The comparison of cell numbers between L- and D-PDMP treatment in CHO-K1 (b) and Z65 (c). The cell numbers were not different in CHO-K1. At 48 h and 72 hr, the cell numbers of Z65 with D-PDMP were significantly smaller than those with L-treatment. Values represent the mean± SD.

Figure 25

Viability assay under exposure to H_2O_2

(a) Viability of CHO-K1 was compared between L- and D-PDMP treatment. There was no significant difference between L- and D-PDMP treatments. At 1.4 mM concentration of H_2O_2 (indicated by dotted line), CHO-K1 under L- or D- PDMP treatment remained around 100% viability. (b) By contrast, only 50% of Z65 under D-treatment survived at 1.4 mM concentration of H_2O_2. The difference of viability was significant at 2.8 mM concentration of H_2O_2 between L- and D-PDMP treatment in Z65 ($p<0.05$).

Figure 26

Attachment assay

(a) The number of CHO-K1 cells attached on laminin and collagen IV were smaller than those of Z65 cells. The number of Z65 on fibronectin was smaller than that of CHO-K1. The differences between CHO-K1 and Z65 did not reach the statistical significance. (b) Cell adhesion between L- and D-PDMP treatment showed no significant difference in CHO-K1. (c) D-PDMP treatment decreased the cell numbers of Z65 attached on laminin, fibronectin and collagen IV, compared to L-PDMP treatment with statistical significance ($p<0.01$).

Figure 27

Immunohistochemistry for ß1-integrin

CHO-K1 and Z65 with or without L- or D-PDMP treatment were seeded on the indicated extracellular matrices and immnostained for ß1-integrin. The staining was weaker in Z65 than in CHO-K1. There is no difference in expression of ß1-integrin

among control (without PDMP treatment), L- or D-PDMP treatment in both CHO-K1 and Z65. Scale bars,10 μ m.

Figure 28

Western blotting for ß1-integrin

(a) Cells treated as in Fig. 27 (C, control; L, L-PDMP; D, D-PDMP) were lysed and Western blotted for ß1-integrin and ß actin (40 and 10 μ g protein per lane, respectively). (b) Relative expression of ß1-integrin in CHO-K1 and Z65 without PDMP treatment. Significant differences were observed in ß1-integrin expression between CHO-K1 and Z65. (c) No significant difference in ß1-integrin expression was shown between L- and D-PDMP treatment both in CHO-K1 and Z65. The differences between CHO-K1 and Z65 under L- or D- PDMP treatment were significant ($p<0.01$).

Figure 29

Possible pathogenic role of increased gangliosides in peroxisomal deficient cells

Integrins are transmembrane receptors that mediate cell attachment to the surroundings. They are also involved in cell signaling, and regulate cell cycle, cell shape and motility. Both ganglioside and ß1-integrin are required for maintenance of plasma membrane microdomains, which may play crucial role in modulating integrin-mediated adhesion [Singh et al., 2010]. An increase of gangliosides may alter the interaction of gangliosides and ß1-integrin, affecting cell adhesion, which in turn alter cell movements in the CNS with ZS.

FIGURES

Figure 1

List of *PEXs* whose mutations give rise to multiple clinical symptoms in ZS and RCDP spectrum

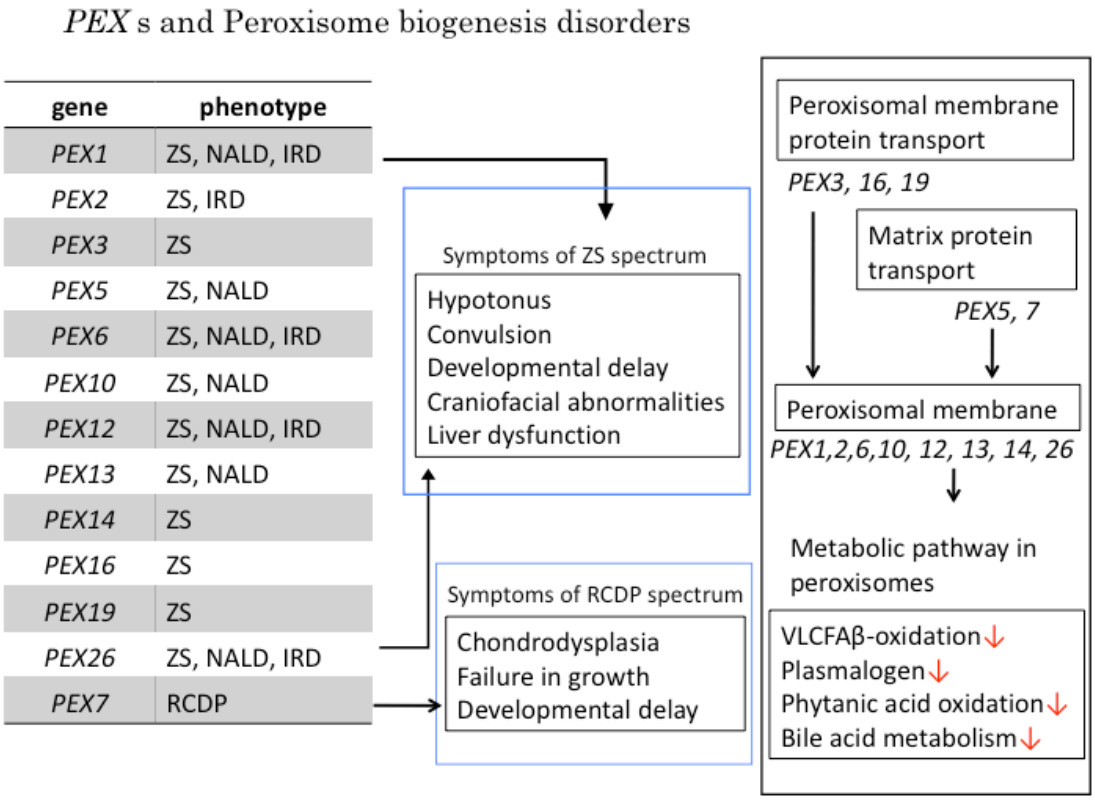

Figure 2

Peroxisomal membrane proteins and matrix import mechanism

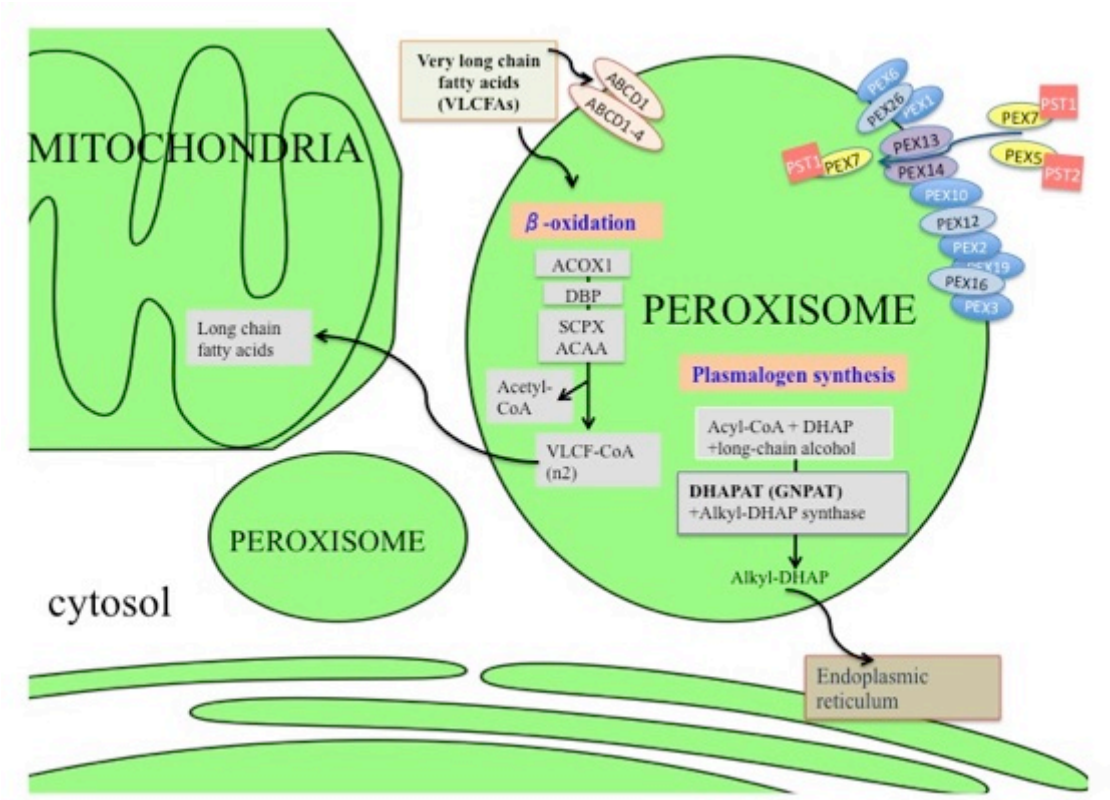

Figure 3

Lipid structures and species

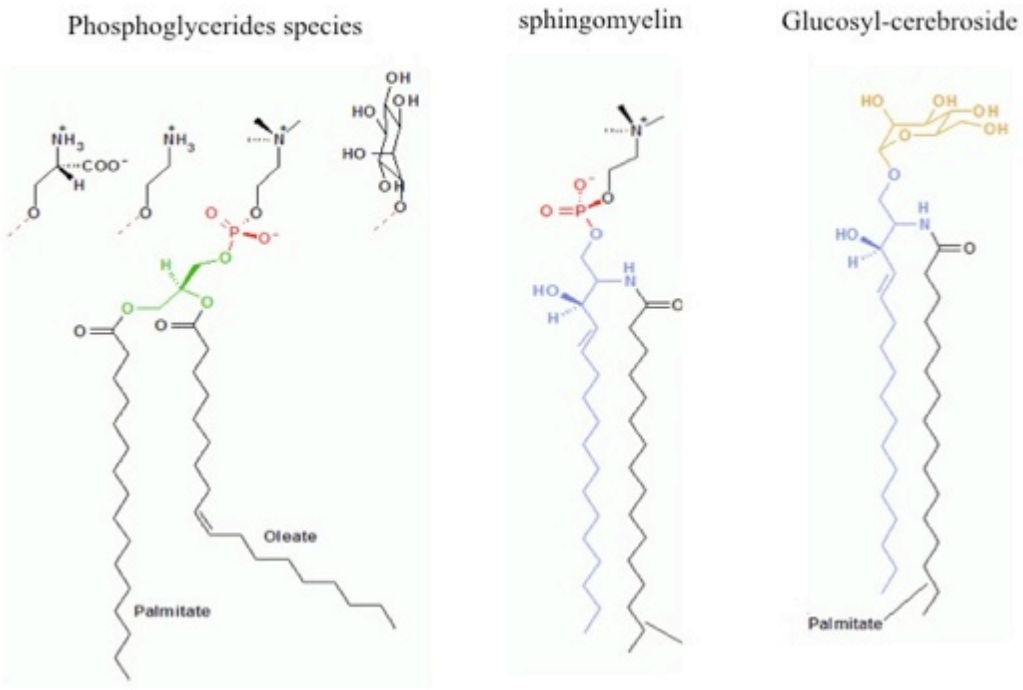

Figure 4

Peroxisomal metabolic pathways

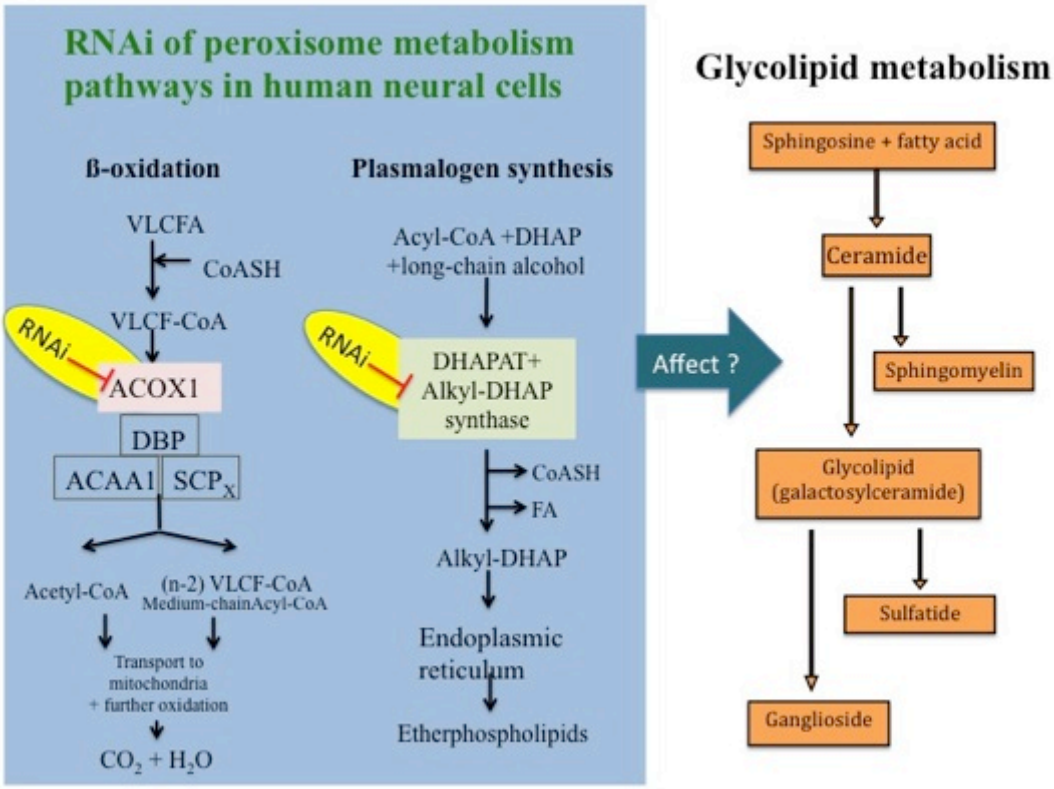

Figure 5

Schema of vector construction of pGE-2-hrGFP II shRNA

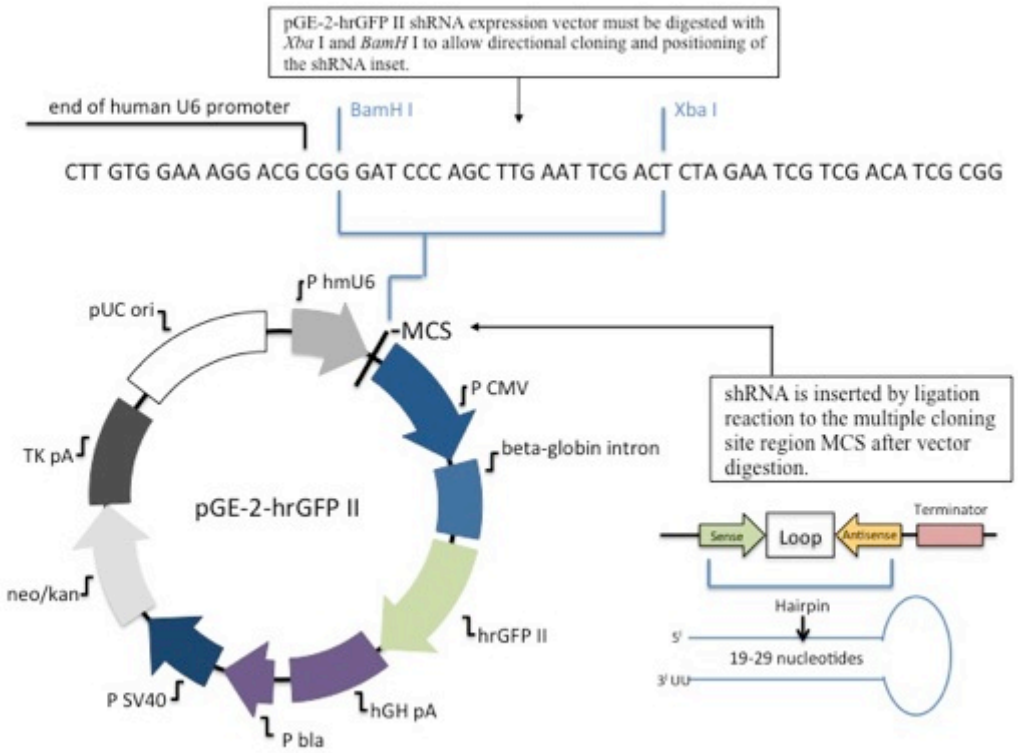

Figure 6

TLC analysis for cholesterol in controls' and patients' cerebellum and cerebrum of grey (G) and white (W) matter samples

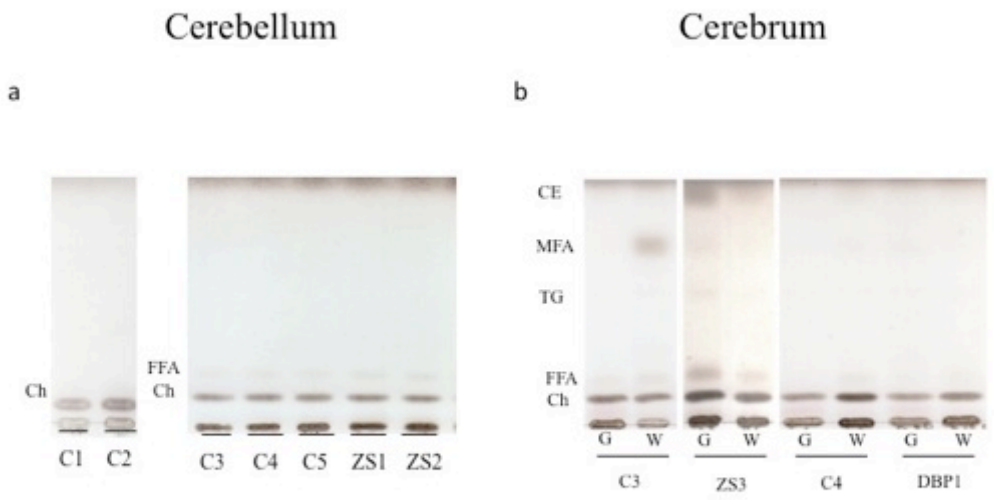

Figure 7

TLC analysis of cholesterol in controls' and patients' liver

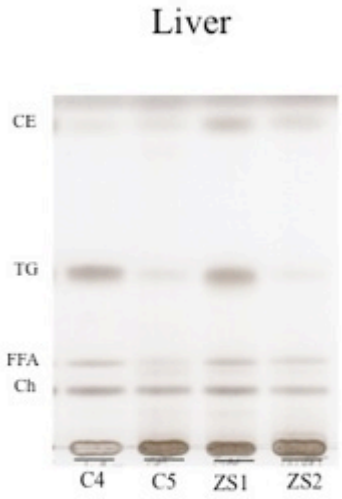

Figure 8

TLC analysis of cholesterol in controls' and patients'fibroblasts

Figure 9

TLC analysis of phospholipids in controls' and patients' cerebellum

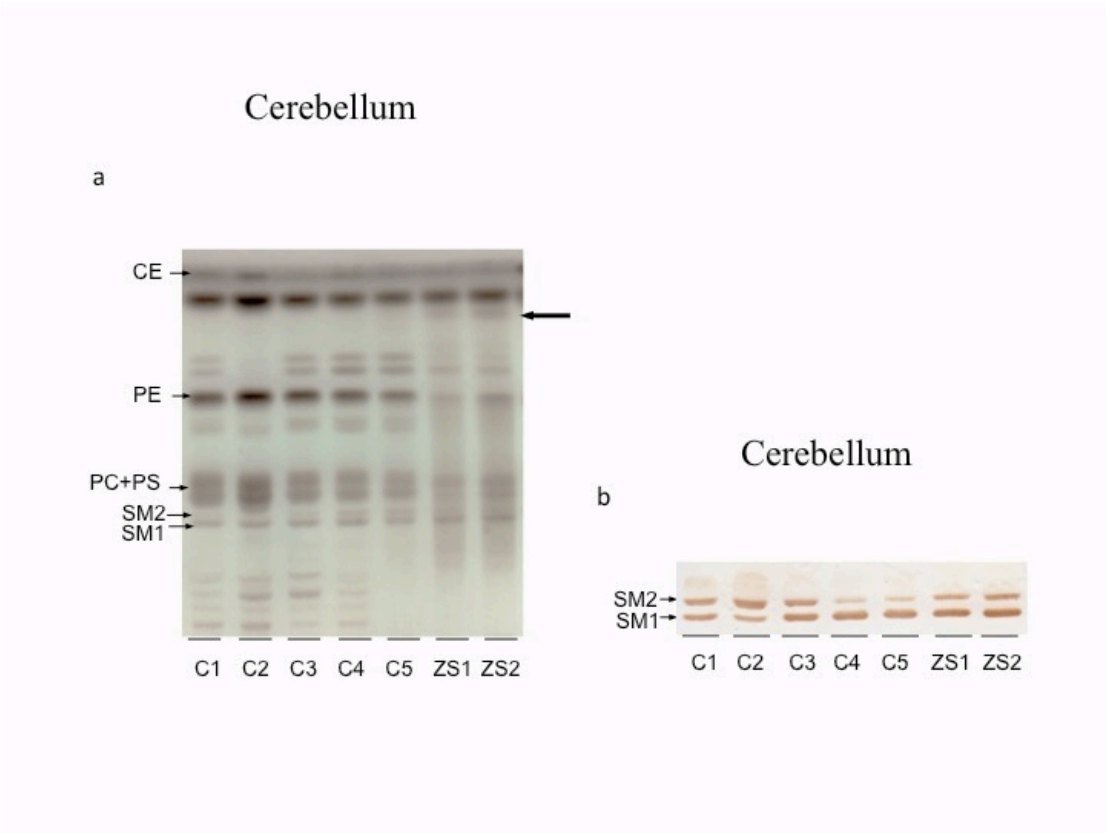

Figure 10

TLC analysis of phospholipids in controls' and patients' liver

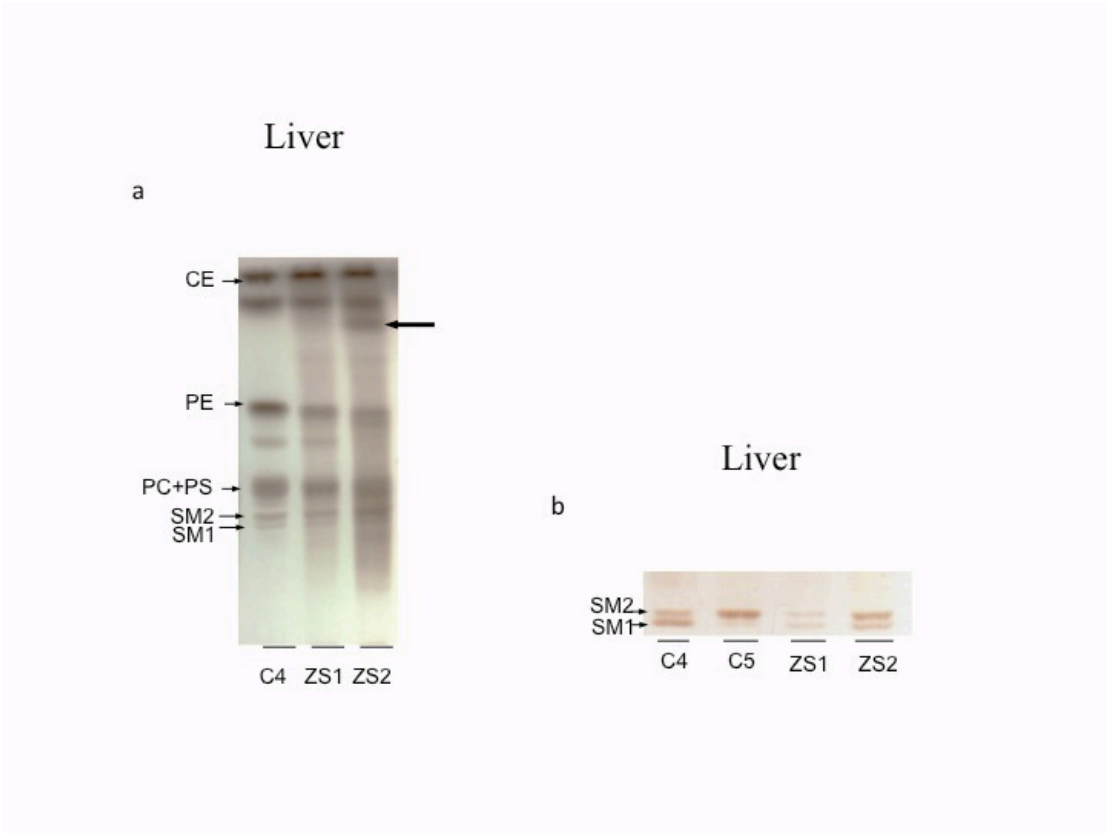

Figure 11

TLC assay for plasmalogen contents before and after HCl treatment in controls' and patients' cerebellum

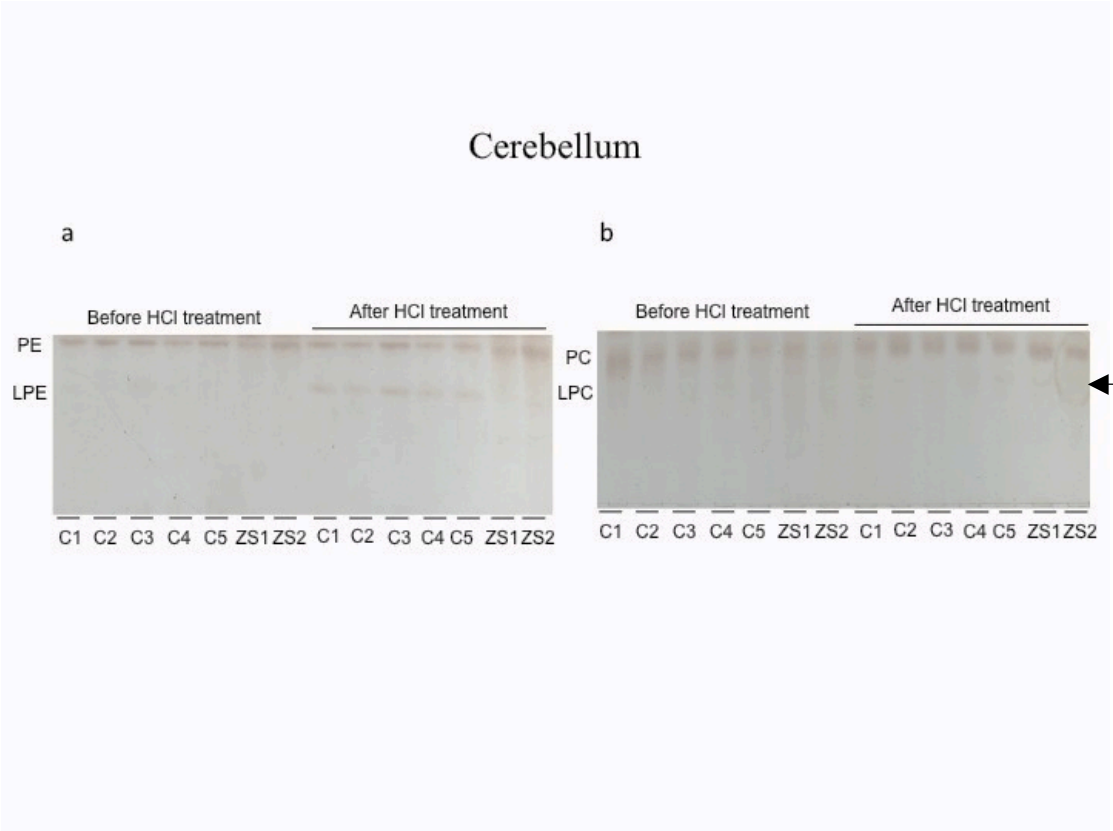

Figure 12

TLC assay for plasmalogen contents before and after HCl treatment in controls' and patients' liver

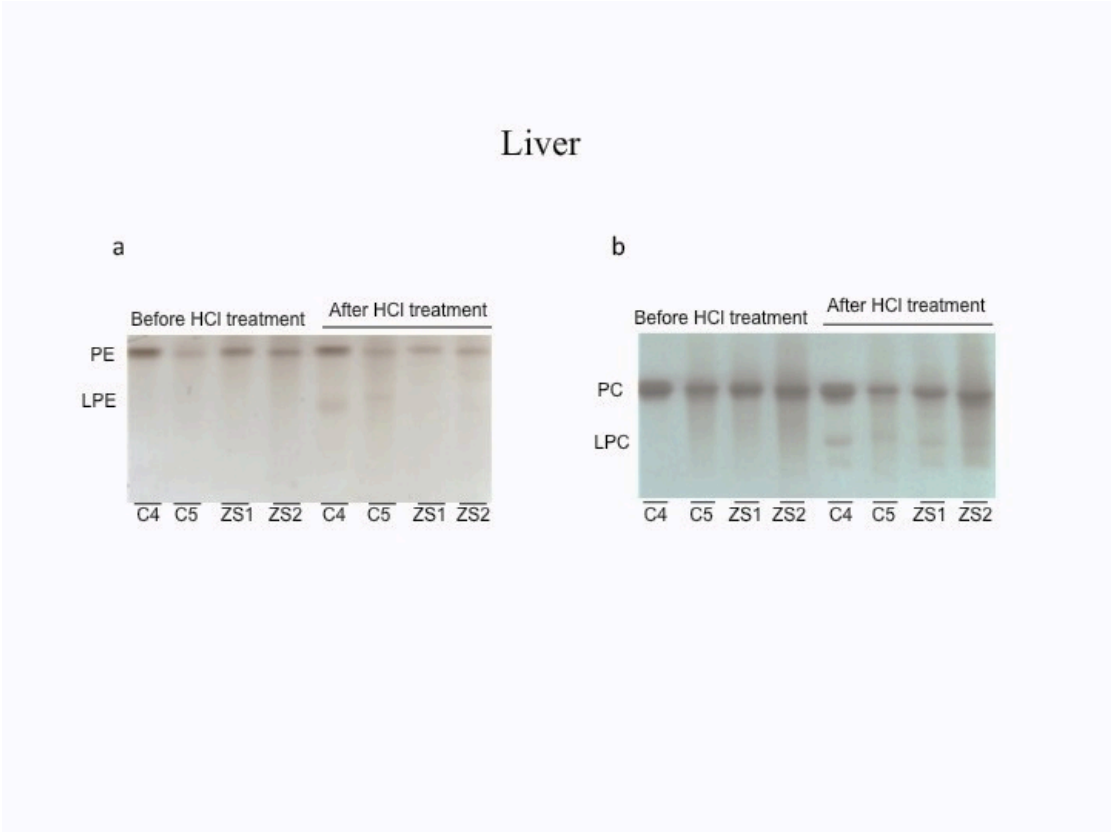

Figure 13

TLC analysis of glycolipids in controls' and patients' and cerebellum and cerebrum of grey and white matter

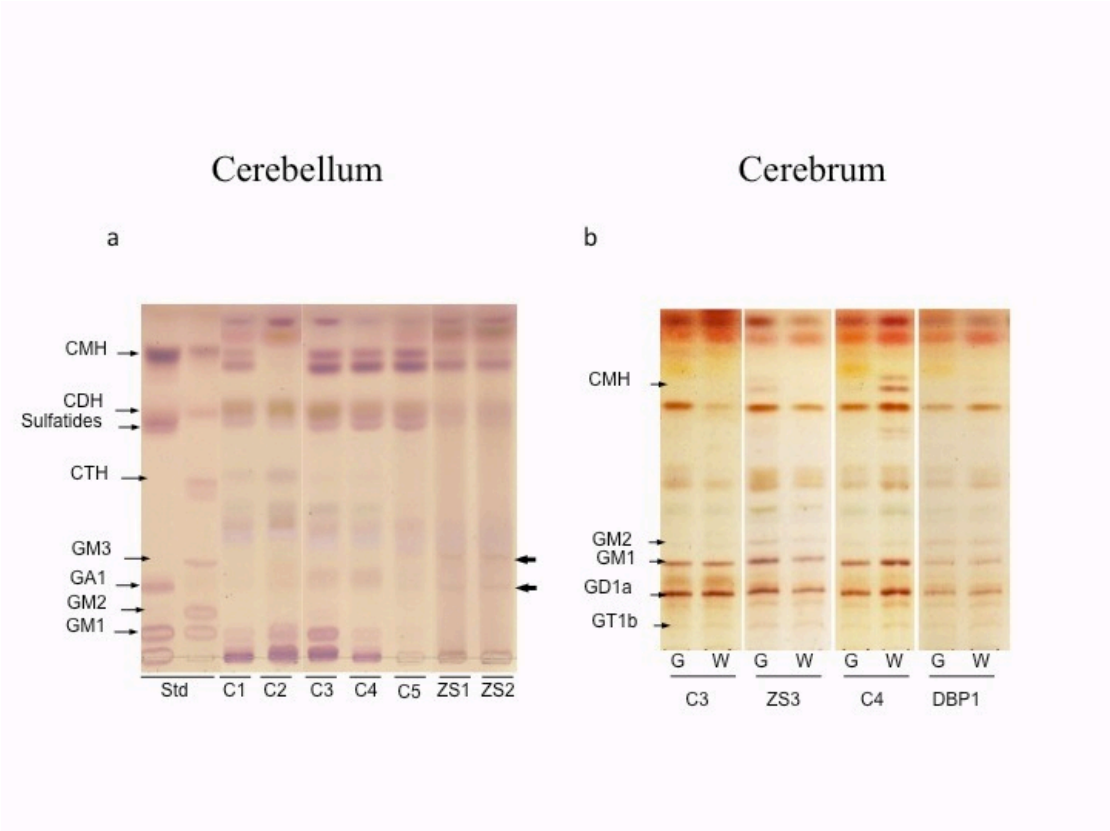

Figure 14

TLC of glycolipids in controls' and patients' fibroblasts

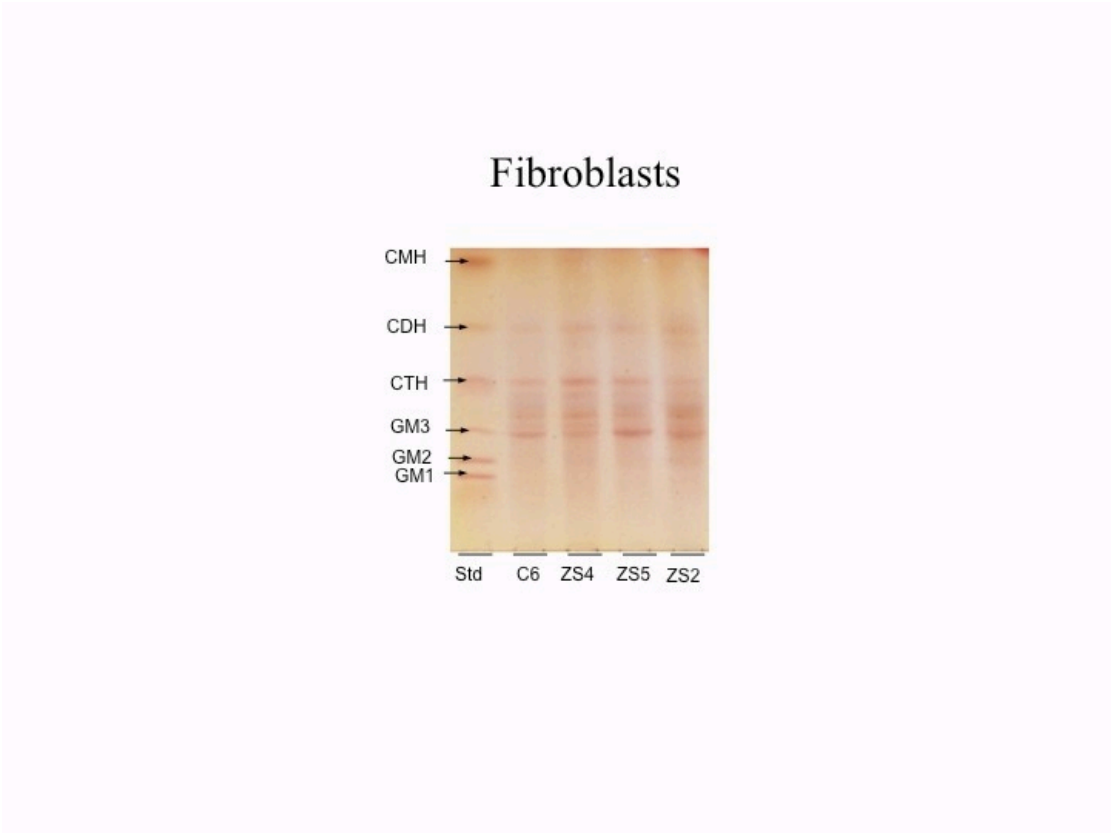

Figure 15

shRNA vector construction

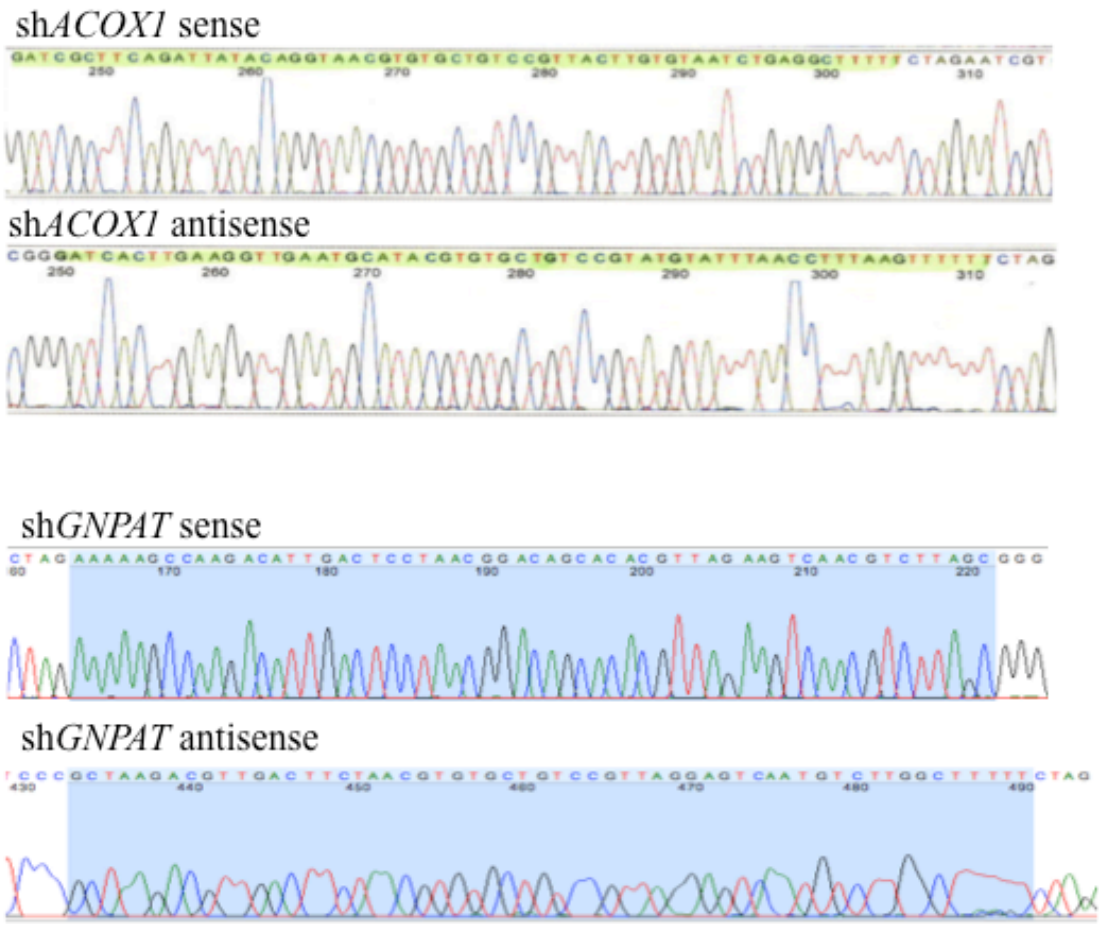

Figure 16

A representative confocal laser microcopy picture of GFP positive transfected cells

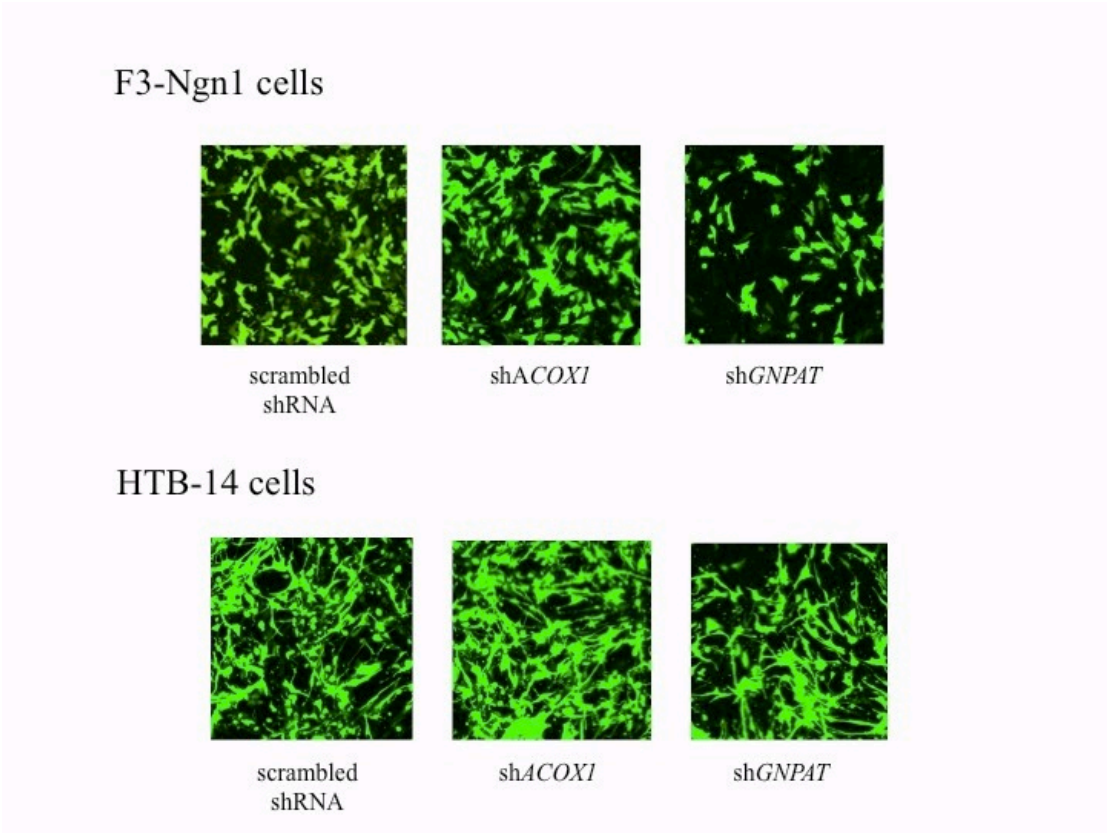

Figure 17

Sorting of F3-Ngn1 and HTB-14 cells transfected with scrambled shRNA

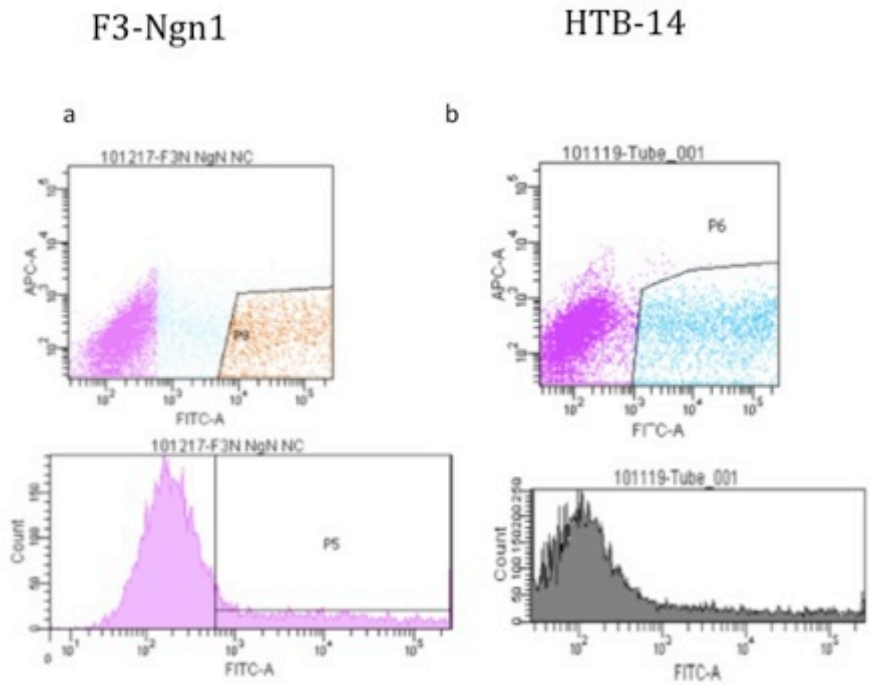

Figure 18

Relative expression of *UGCG* and *UGT8* in A*COX1* and *GNPAT* RNAi F3-Ngn1 and HTB-14 cells

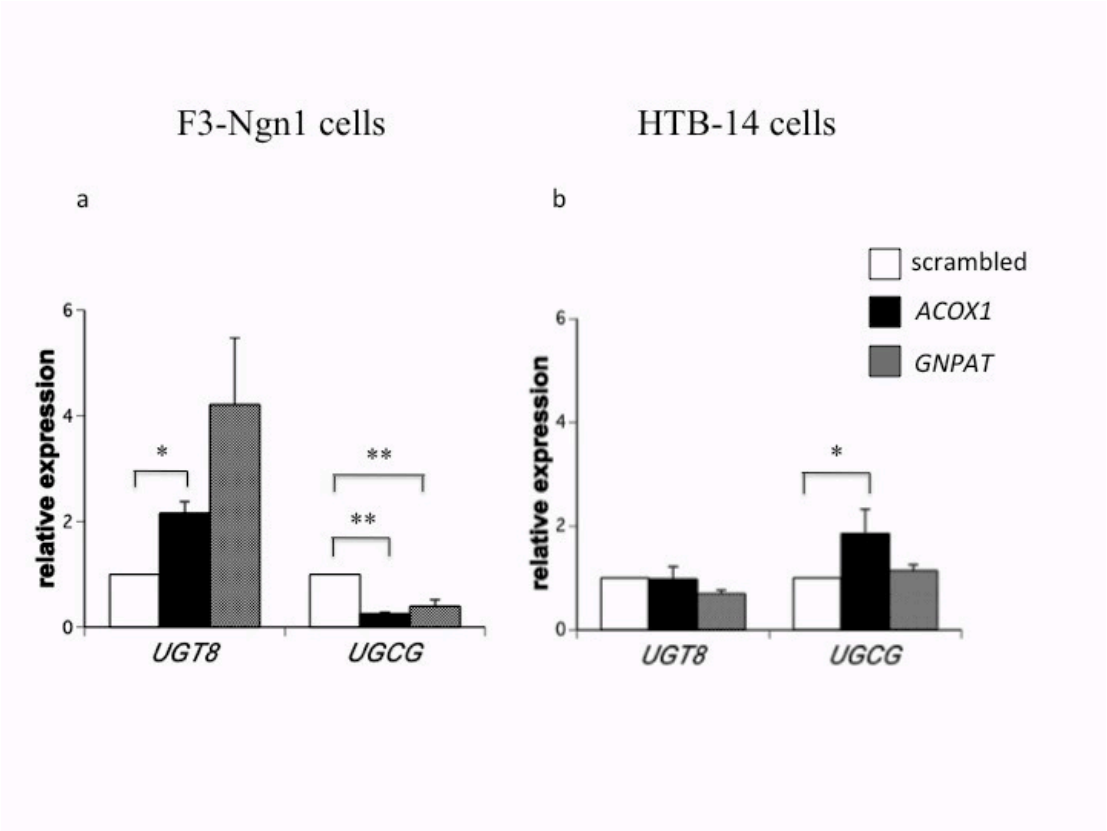

Figure 19

Summary of altered glycolipids regulation in DBP and ZS patients

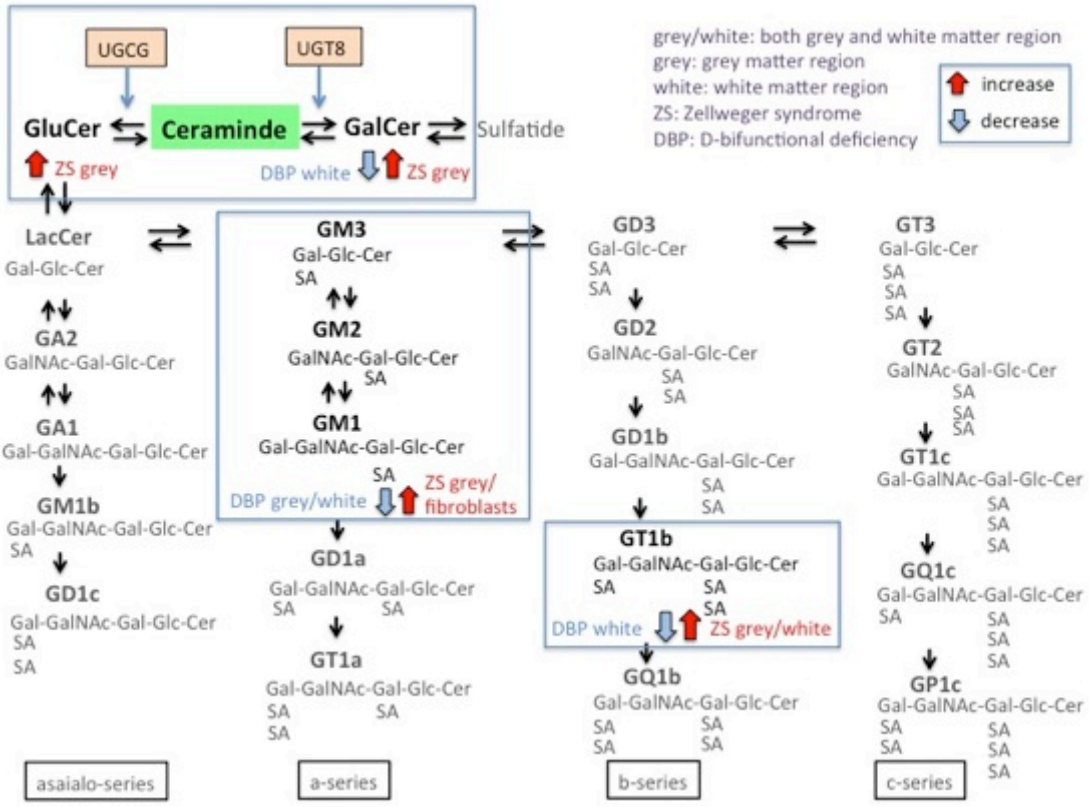

Figure 20

The import of peroxisomal matrix proteins through the peroxisome membrane assembly

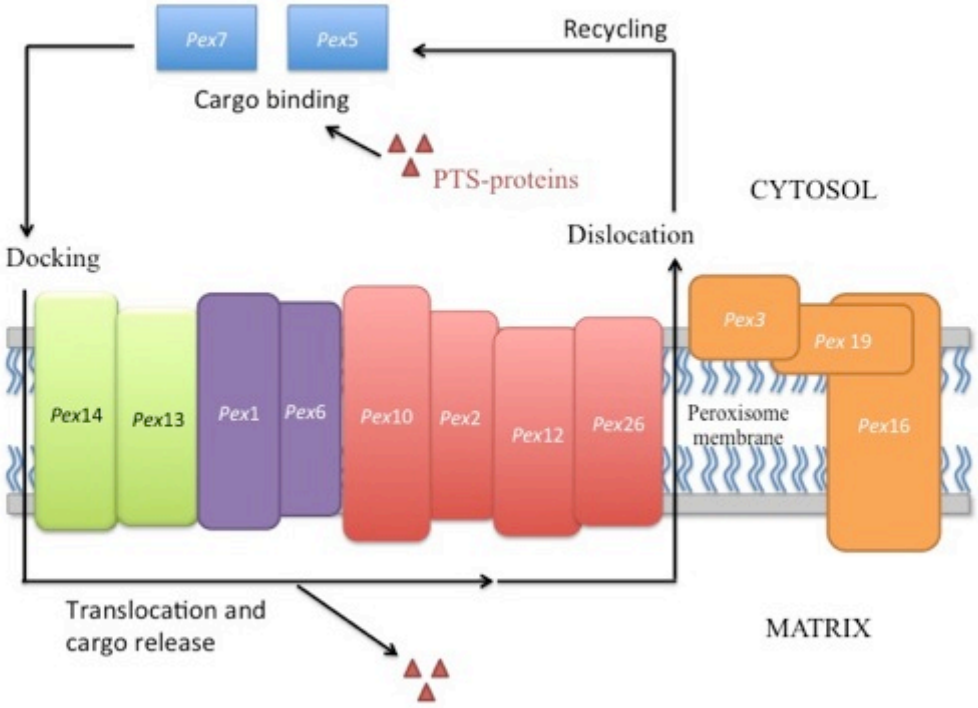

Figure 21

***Pex2* mutant Chinese hamster ovary cells (Z65)**

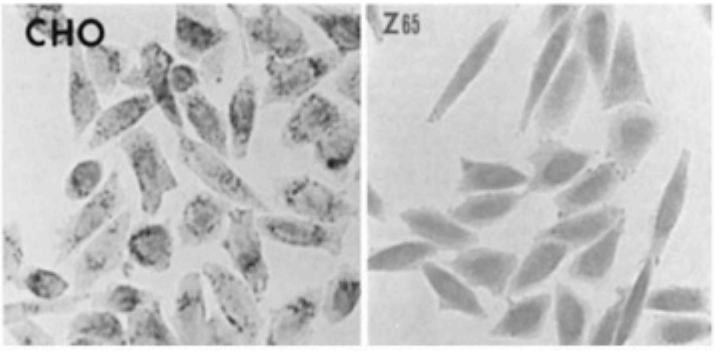

Tsukamoto, et al. 1990 J Cell Biology

21

Figure 22

Structure of L-PDMP and its enantiomer D-PDMP

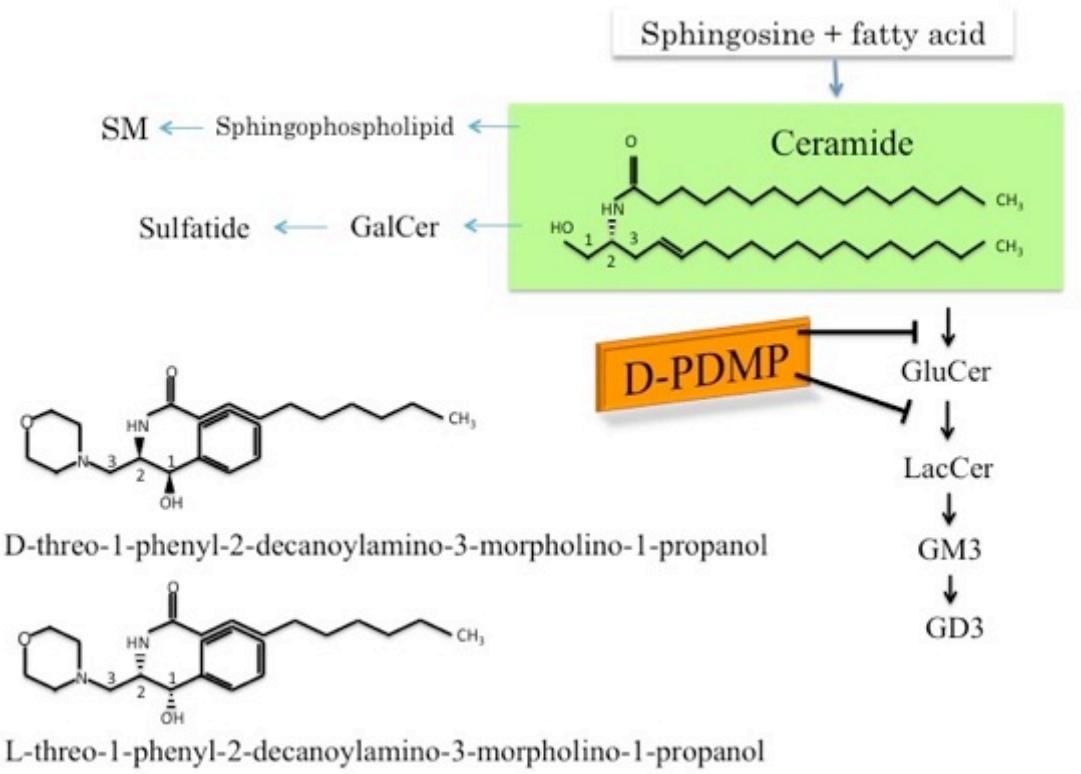

Figure 23

TLC analysis of glycolipids for CHO-K1 and Z65

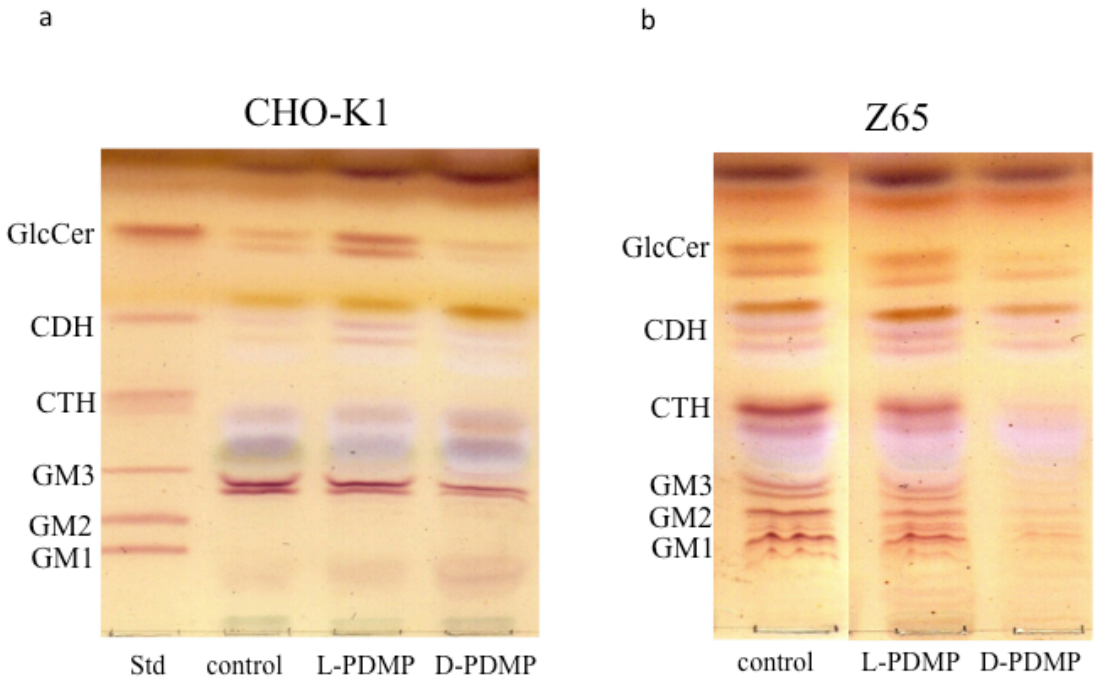

Figure 24

Effect of L- and D-PDMP on CHO-K1 and Z65 proliferation

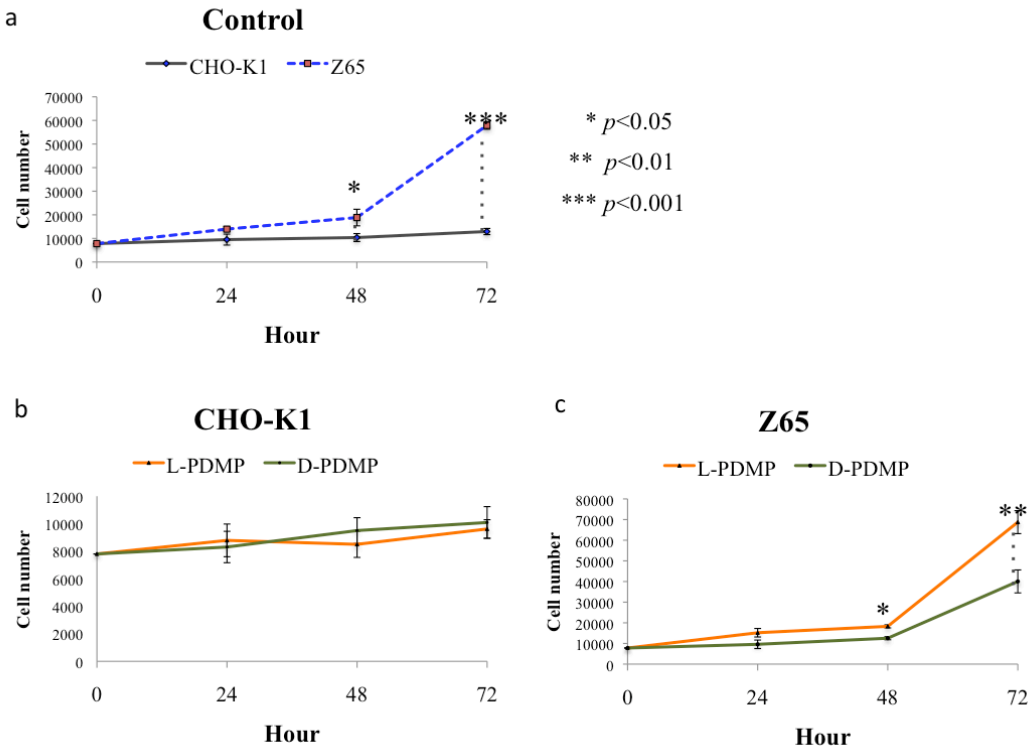

Figure 25

Viability assay under exposure to H_2O_2

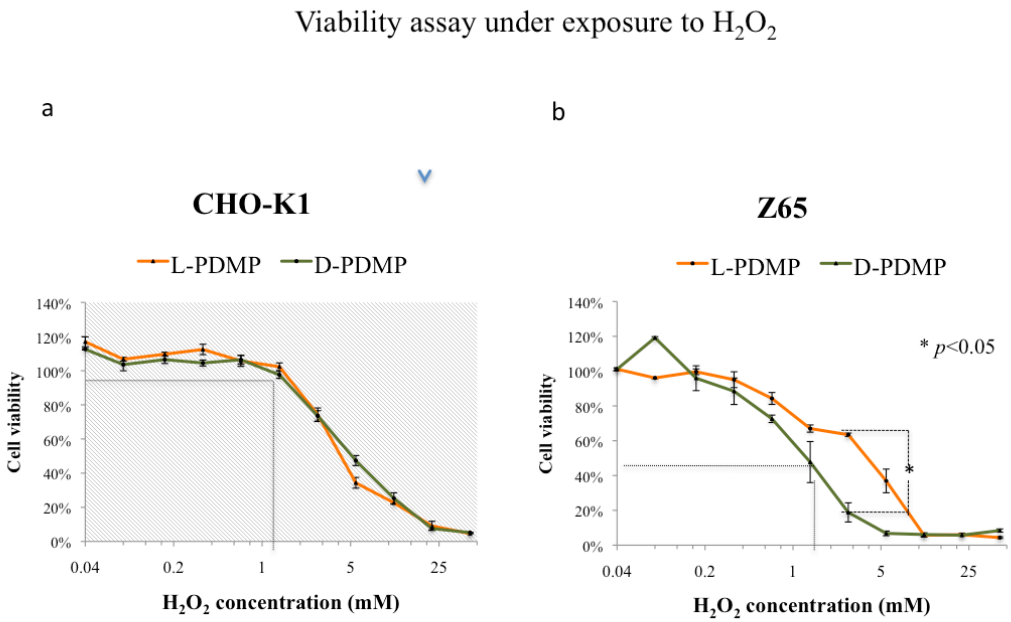

Figure 26

Attachment assay

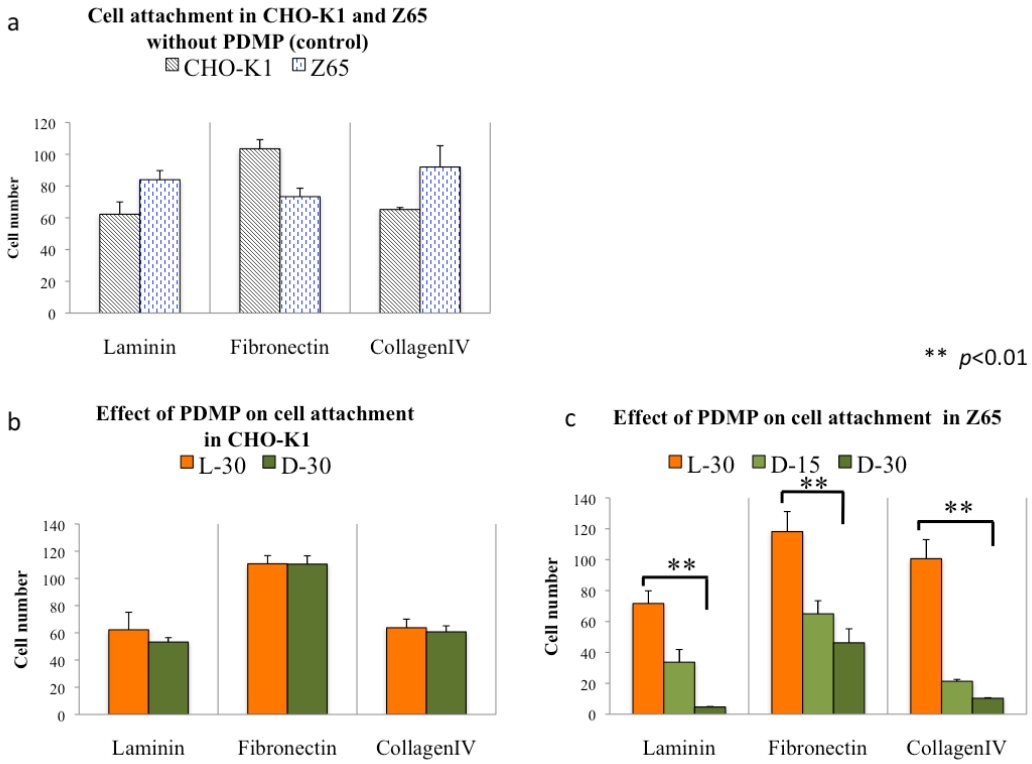

Figure 27

Immnohistochemistry for ß1-integrin

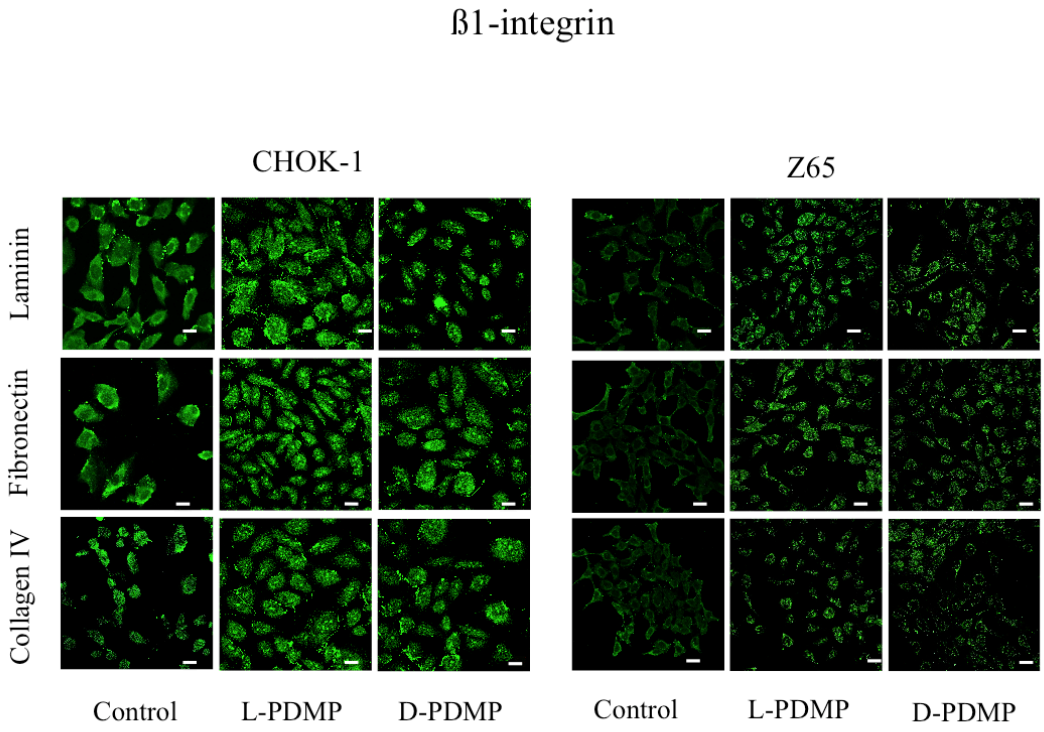

Figure 28

Western Blotting for ß1-integrin

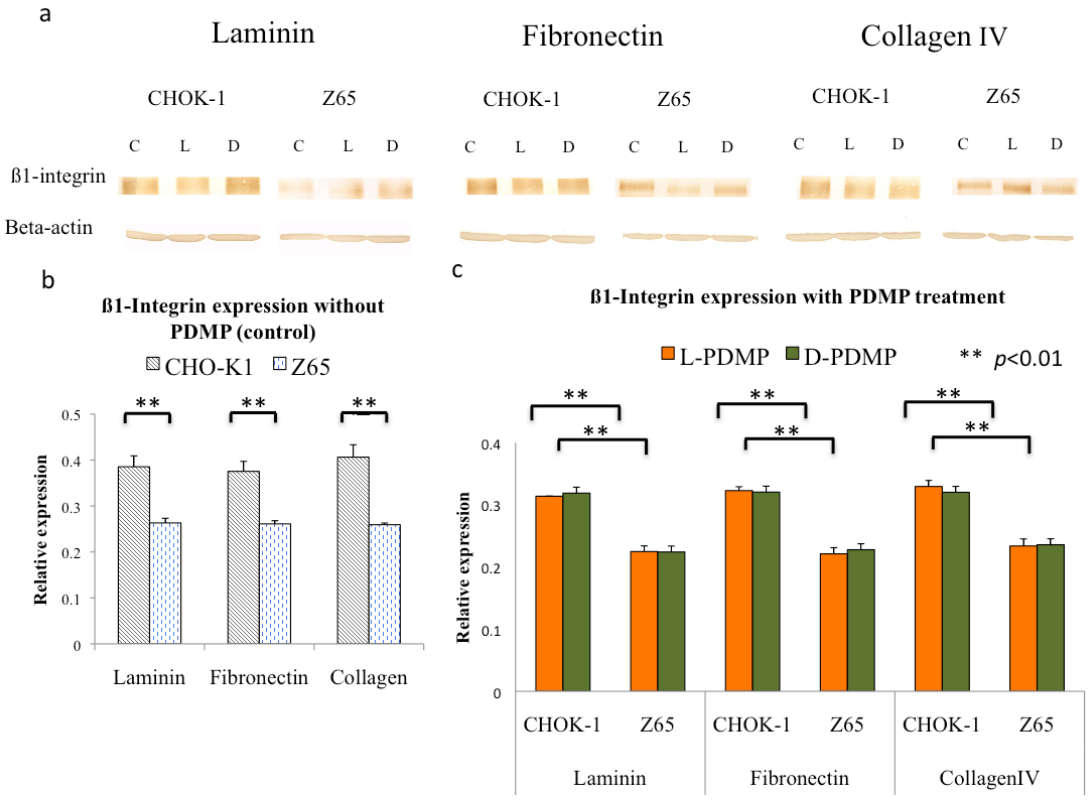

Figure 29

Possible pathogenic role of increased gangliosides in peroxisomal deficient cells

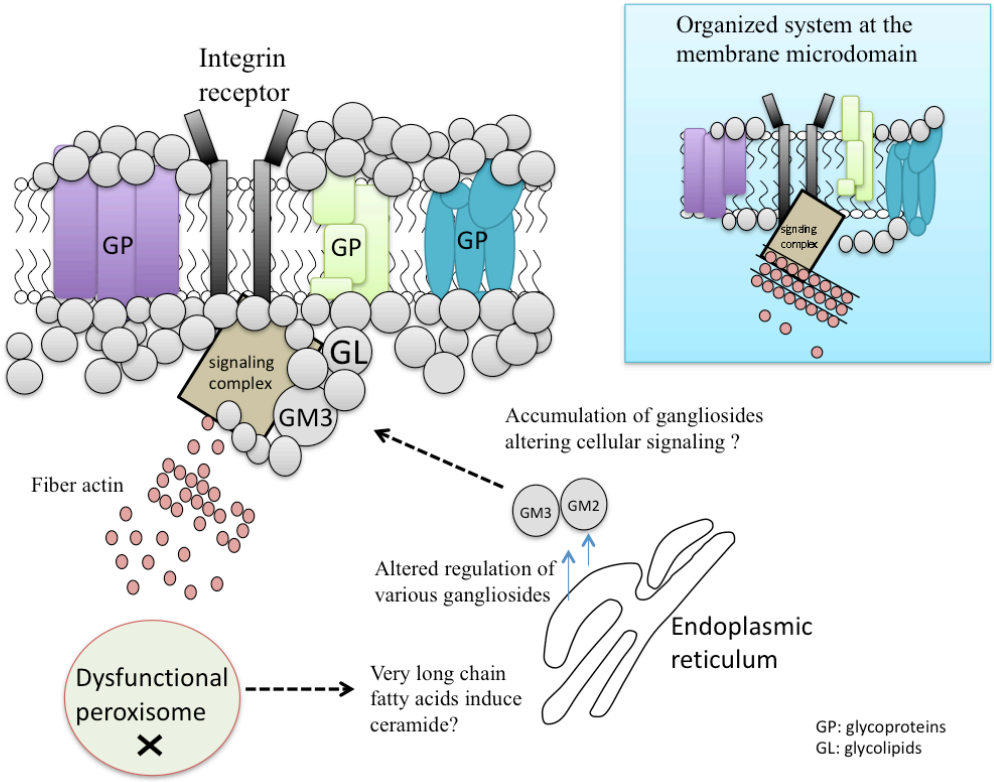

TABLES

Table 1

Samples of patients with peroxisomal disorders and controls

Patients	Mutated genes	Age, Sex	Samples
ZS1 (US)	*PEX 26*	6 months, Female	Cerebellum; Liver
ZS2 (US)	*PEX 1*	7 months, Female	Cerebellum; Liver; Fibroblasts
ZS3 (JP)	NI	7 months, Male	Frontal lobe grey and white matter
ZS4 (US)	*PEX 5*	NA	Fibroblasts
ZS5 (US)	*PEX 5*	NA	Fibroblasts
DBP (JP)	*HSD17B4*	1 year and 7 month, Male	Frontal lobe grey and white matter
Controls	Cause of Death	Age, Sex	Samples
C1 (JP)	Micrognathia	0 year, Female	Cerebellum
C2 (JP)	Respiratory distress Syndrome	0 year, Male	Cerebellum
C3 (JP)	Sudden infant death syndrome	6 months, Female	Cerebellum; Frontal lobe grey and white matter
C4 (JP)	Sudden infant death syndrome	1year and 9 months, Male	Cerebellum; Frontal lobe grey and white matter; Liver
C5 (US)	Burn	6 years, Male	Cerebellum; Liver
C6 (US)	-	2 months, Male	Fibroblasts

(US) Samples were obtained received from Peroxisomal Diseases Lab, Kennedy Krieger Institute, Baltimore, United States and NICHD Brain and Tissue Bank at the University of MD. (JP) Samples were originated from Japanese patients. NI; not identified, NA; not available

Table 2

The sequence for shRNA and RT-PCR primers

	sense	antisense
*ACOX1*shRNA	5′GCCTCAGATTACACAAGTAAA3′	5′TTTACTTGTGTAATCTGAGGC3′
*GNPAT*shRNA	5′GCCAAGACATTGACTCCTAAA3′	5′TTTAGGAGTCAATTGTCTTGGC3′
UGCG	5′TGGAAACATTCTTTGAATTGGA3′	5′CGTGAACCAAGCCTACTTTTTC3′
UGT8	5′CGCTACCCAGGGATCTTTAAC3′	5′ACCCACTTCAGCAGGATACC3′
G6PDH	5′CCGATTACTACGCCTACAGC3′	5′GCCGCTACTGAACTCAAACT3′

The sequences for shRNA of *ACOX1* and *GNPAT* and primer sequences for RT-PCR are shown.

Table 3

Amount of cholesterol in patients' and controls' brain, liver and fibroblasts.

A

Cerebellum

Patients	Amount of total lipid applied (µl)	Amount of cholestrol in total lipid (µg)
ZS1*	5	1.34
ZS2*	5	1
Controls		
C1**	5	1.35
C2**	5	1.33
C3**	5	1.62
C4**	5	1.67
C5*	5	1.9

b

Cerebrum

Patients	Amount of total lipid applied (µl)	Amount of cholestrol in total lipid of grey matter (µg)	Amount of cholestrol in total lipid of white matter (µg)
ZS3**	10	1.48	0.75
DBP**	10	0.65	0.84
Controls			
C3**	10	0.93	0.81
C4**	10	0.72	1.32

C

Liver

Patients	Amount of total lipid applied (µl)	Amount of cholestrol in total lipid (µg)
ZS1*	10	1.34
ZS2*	10	0.8
Controls		
C4**	10	1.42
C5*	10	1.19

d

Fibroblasts

Patients	Amount of total lipid applied (µl)	Amount of cholestrol in total lipid (µg)
ZS4*	20	0.3
ZS5*	20	0.2
ZS2*	20	0.2
Control		
C6*	20	0.4

Amount of cholesterol in total lipid extract from *lipid weight and **tissue dry weight of cerebellum, cerebrum, liver and fibroblast of normal controls and DBP and ZS patients.

Table 4

Amount of phospholipids in cerebellum of normal controls and patients with ZS

	Control (n=3)*	ZS1	ZS2
PE	7.173±1.292	1.766	3.077
PC+PS	5.497±1.577	2.353	3.809
SM1	0.725±0.193	1.233	1.623
SM2	0.746±0.318	0.425	0.654
SM1/SM2	0.972±0.105	2.900	2.479

Amount of lipids in cerebellum of normal controls and the patients with ZS. Values are microgram/1microgram cholesterol. The measuament of SM1/ SM2 was performed with TLC immunostaining results. * The amount of controls (under 1 year old) is presented mean as a value±SD of three samples (C1, C4 and C5).

ACKNOWLEDGEMENTS

I would like to present my most sincere gratitude towards the patients and their families for participating in this study. My dream of contributing to the science research community is only made possible with Professor Masashi Mizuguchi and Dr. Makiko Saitoh' s exceptional teaching, advices, and constant support throughout my years at the Department of Developmental Medical Sciences, School of International Health, the University of Tokyo. Deep appreciation is also imparted to Dr. Masao Iwamori, Dr. Makoto Miyagishi, Dr. Ann B. Moser at Peroxisomal Diseases Lab, Kennedy Krieger Institute, Baltimore, United States, and NICHD Brain and Tissue Bank at the University of MD for their contributions to this study. "*So shall the knowledge of wisdom be unto thy soul: when thou hast found it, then there shall be a reward, and thy expectation shall not be cut off." (Proverbs 24:14) KJV*